Dielectric and Magnetic Properties of Pure and Doped Cobalt Ferrite Nanoparticles

By

Amr Min Allah

School of Chemical and Materials Engineering

National University of Sciences and Technology

2021

Dielectric and Magnetic Properties of Pure and Doped Cobalt Ferrite Nanoparticles

Name: Amr Min Allah

Reg. No: NUST 2017 NSE-05-00000204434

This thesis is submitted as partial fulfillment of the requirements for the degree of

MS in (Nano Science and Engineering)

Supervisor Name: Dr. Iftikhar Hussain Gul

School of Chemical and Materials Engineering (SCME)

National University of Sciences and Technology (NUST)

H-12 Islamabad, Pakistan

2021

Dedication

*“I dedicate this thesis to my **Parents** for their love, support, affection and prays of the day and night make me able to achieve such success and honour”*

Acknowledgments

All admiration to Allah Almighty who is the creator, maintainer, and the Regulator of the world. He is the One, who bestows and gives the power to us to think, utilize our expertise in knowledge in achieving remarkable solutions for mankind in every field. Therefore, I express my greatest thanks to Almighty Allah the universal and the architect of the world, who has gifted us the brain and instable nature construction of knowledge and body to achieve our work in the form of this project report. As Allah Almighty says in Quran:
"Read! In the name of your lord" (Alaq; 1st revealed ayah).

This Quranic verse sums up the entire importance of education in the lives of humans. I like to express my gratefulness to my very nice and respected supervisors Dr. I H Gul, Dr. Aftab Akram my GEC Members Dr. Nasir and Dr. Sofia javed and for their clear and patient guidance that directed me to fulfil my project and this thesis. Their cool and calm behaviour motivated me to do my best. Their valuable suggestions and feedback contributed greatly to this thesis. Also, I am very grateful to all my teachers who helped me and motivated me to do the best. I would also like to thank my parents, family members, and friends for their help, prayers, and their valuable suggestions.

I am thankful to all the faculty members to build my basis of Nano Science and Engineering. I want to thank Ms. Sidra Tul Muntha, Mr. Mutawara Baig, Mr. Muhammad Zarar, Ms. Saira Qayyum, for their continuous support and motivation which helped me at various stages during my Masters.

I acknowledge the support provided by the Materials Engineering Department of SCME for providing me a platform to perform my experiments and using my skills in research work. I feel honoured to thank all the lab engineers, especially those who assisted me in all the possible manners.

I acknowledge the financial aid and technical assistance provided by our department, SCME, during my research experience and made this project work memorable forever. Last, but not the least, I want to thank my family and in laws for their prayers, support, and confidence in me without which I would not have been able to reach my full potential.

-Amr Min Allah

ABSTRACT

The exceptionally unique magnetic and electric properties of ferrites have always been of strong interest leading to their extensive commercial use. Cobalt ferrite is one of the materials being used in microwave, electronic and magnetic devices. In present research study Nickel, Zinc, Magnesium and Manganese substitution is performed in a series of $Co_{0.5}(Ni, Zn, Mg, Mn)_{0.5}$ Fe_2O_4.Synthesis was performed using sol gel method and aqueous solutions of nitrates were used to prepare pure and doped Cobalt Ferrite nanoparticles. Calcination of the prepared samples was performed at 950 ^oC for 3 hours. The samples were characterized using X-ray Diffraction (XRD), Scanning electron microscopy and Fourier transform Infrared spectroscopy. Impedance analyser was used to analyse the dielectric properties. Magnetic properties of the samples were studied using Vibrating Sample Magnetometer. XRD analysis confirms the Spinel crystal structure of prepared. Crystallite size was calculated using Debye Scherer formula and it came out in the range of 26 nm- 38nm. Vibrating band positions were studied using FTIR. Dielectric studies revealed high value at low frequency while decreases with increasing frequency in dielectric constant. Similarly, the dielectric loss value was high for low frequency while small for high frequency. While value of tangent loss decreases with increasing frequency. The AC conductivity is maximum at higher frequency which represents the dominance of hoping conductivity over band conductivity. While Ac impedance shows decreasing trend in Ac impedance with increasing frequency. While for Electric Modulus it is shown that in low frequency region the M' value is very low (approaching to zero) while with increasing frequency its value increases and approaches to maximum asymptotic value for all samples.

VSM shows increase in saturation magnetization for cobalt nickel ferrite while it decreases for other samples. For pure Cobalt ferrite, the Mr= 19.34emu/g. while its value increases for Cobalt Nickel ferrite and Cobalt Zinc ferrite (43.32 emu/g, 24.34 emu/g). While decreases for Cobalt magnesium ferrite and Cobalt Manganese ferrite (17.9 emu/g, 17.34 emu/g) . The **Coercivity** value increases for the dopants as compare to pure cobalt ferrite.

Table of Content

List of Figures

List of Tables

LIST OF ABBREVIATIONS

$CoFe_2O_4$……. Cobalt Ferrite

$CoNiFe_2O_4$ …… Cobalt Nickel Ferrite

$CoZnFe_2O_4$……. Cobalt Zinc Ferrite

$CoMgFe_2O_4$……... Cobalt Magnesium Ferrite

$CoMnFe_2O_4$…… Cobalt Manganese Ferrite

XRD…….. X-Ray Diffraction

SEM…….. Scanning Electron Microscopy

EDX..…… Energy Dispersive X-Ray Analysis

FTIR……...Fourier Transform Infrared Spectroscopy

VSM…….. Vibrating Sample Magnetometer

(CHAPTER 01)

1. INTRODUCTION

Nano materials are the materials having one dimension smaller than 100nm.
They are divided into four types zero, one, two and three dimensional while spherical nanoparticles are zero dimensional, coatings and thin films are one dimensional, nanowires and nanotubes are two dimensional and precipitates and quantum dots are the example of three dimensional. Two important factors that differentiate nanoparticles from bulk materials are large surface area and quantum effect. Due to these factors the property of material enhances like magnetic, electrical and mechanical properties and reactivity due to large surface area.[1]

1.1 Magnetism:

An atom is one of the main building unit of all in the universe and it is made up of electrons, protons and neutrons. Electrons move around the nucleus in orbits and also spin around its own axis. Electrons motion produces small amount of current and due to this changing current causes a magnetic field. The magnetic moment in the magnetic field is always along its axis of rotation. The other magnetic moment electron's spin motion in up or down direction. Magnetic moment is zero for fully filled shells but for unfilled shell it always has some value. [2]

1.2 Classification of Magnetic Material:

There are few types of magnetic materials depending upon their magnetic behaviour. The most well-known types of magnetism are

- Diamagnetism
- Paramagnetism
- Ferromagnetism
- Anti-ferromagnetism [2]

1.2.1 Diamagnetism

The diamagnetic material will not show any effect without magnetic field. When an electric field is added the spinning electrons arrange in opposite direction to given field and leads to zero net magnetic moment. Magnetic field produced by atom's orbital motion opposes the applied magnetic field called negative susceptibility. The diamagnetic material when placed in non-uniform magnetic field move where the magnetic field strength is weak. [3]

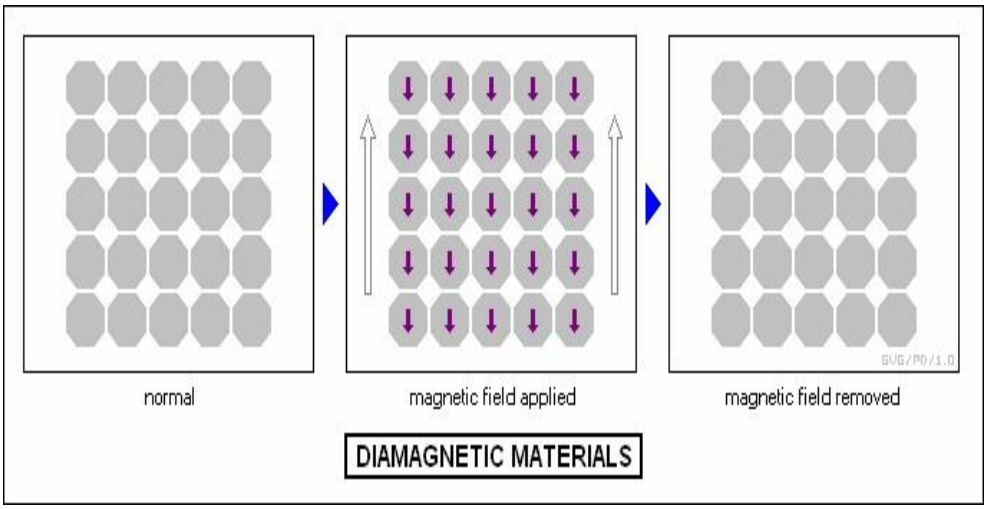

Fig 1.1 Atomic dipole ordering of diamagnetic material [5]

1.2.2. Paramagnetism

When spin and orbital magnetic moment does not completely cancel each other's effect creates permanent dipole moments which results in paramagnetism. The dipoles are randomly aligned without magnetic field and gives zero magnetization when the field is applied the dipoles arranged themselves along the field results in net magnetization. [4]

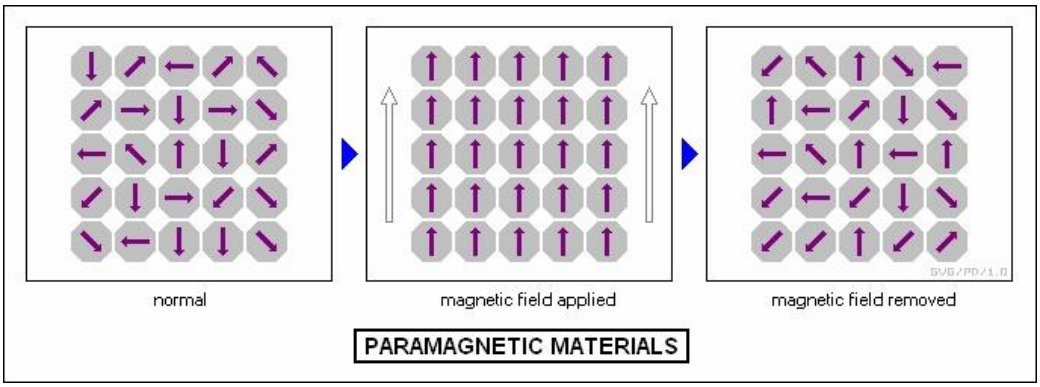

Fig 1.2 Atomic dipole ordering of paramagnetic material. [5]

1.2.3 Ferromagnetism

Ferromagnetism is a phenomena in which magnetic moment of atoms interact and align themselves parallel to each other because of magnetic field present in a material. Their inbuilt field is enough to magnetize the material to saturation so external magnetic field is not required. Iron, cobalt and nickel are the elements that mostly show the ferromagnetic behaviour at and above room temperature these materials become paramagnetic at high temperature called curie temperature. [2]

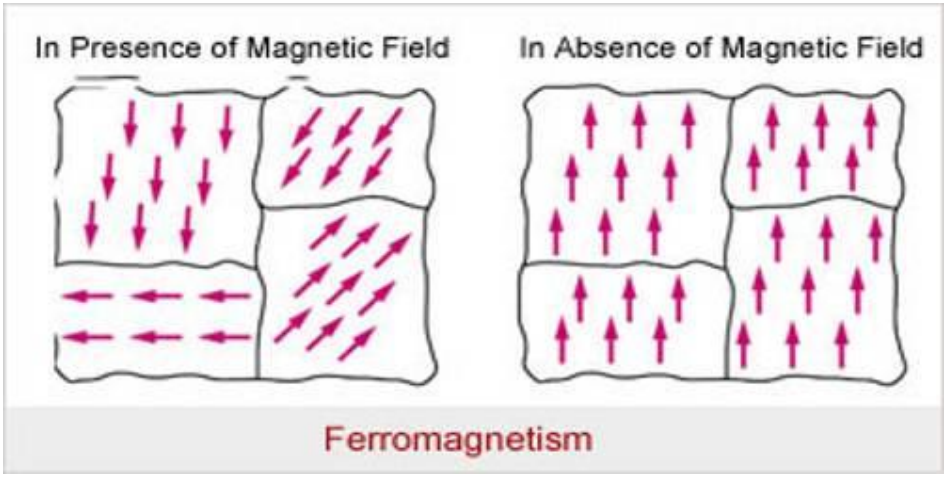

Fig 1.3 Atomic dipole ordering of ferromagnetic material.[69]

1.2.4 Anti ferromagnetism

Antiferromagnetism is almost same as the ferromagnetism. In antiferromagnetism the magnetic moment have the anti-parallel alignment of them as parallel in ferromagnetism and in result becomes diamagnetic material by cancelling each other's effect. Chromium is only example that shows antiferromagnetic behaviour at room temperature. At temperature above

transition temperature this material converts to paramagnetic due to increase in thermal movements so this behaviour is also temperature dependent. And in this phenomena this temperature is called ***NEEL*** temperature.[2]

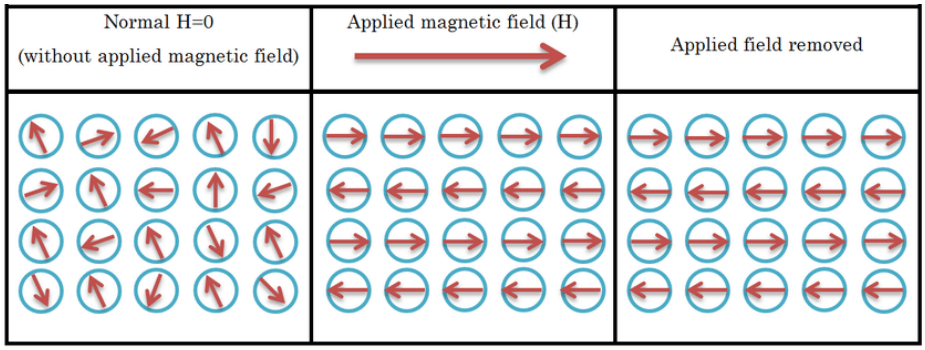

Fig 1.4 Atomic dipole ordering of ferromagnetic material.[70]

1.3 Ferrites:

Ferrites are represented generally as any magnetic oxide in which iron oxide is the main component of their crystal structure.Fe_3O_4, also called magnetite, is known for the first ever magnetic material recognized and was known as load stone. Ferrites have the significant importance among other magnetic materials that were discovered later. They exist in Ferrimagnetic cubic spinel assembly and have both the magnetic materials and electrical insulators nature. Their properties changes at significant level below critical size and due to which Nano ferrites have appreciable importance for their use in devices.

1.3.1 History of ferrites:

The naturally occurring ferrites (Fe_3O_4) caused the scientific interest in humans. People of 600 B.C. In 1890 Du-Bois done the first magnetic measurement of magnetite. While Hilpert in 1909 was the first to prepare ferrites having general formula $MOFe_2O_4$ where M represents divalent metal ion and O representing the oxygen.[2]

The inverted spinel structure of magnetic particles was first discovered by Barth and Posanjak through X-ray analysis. In 1930 huge work on ferrites was done in Holland and the importance of oxygen content for ferrites quality used at high frequency.[6] The ferrites having inverted spinel structure were considered to be ferrimagnetic while normal spinel structure ferrite as nonmagnetic.

In 1948 theory on origin of magnetism in ferrites was proposed by Neel.[7] Later on the two scientists, Gorter and Gaillard, confirmed the theory of Neel by measuring the magnetization of the mixed ferrites. With the assistance of neutron diffraction

studies, Shull and Strauser approved the theory of Neel for magnetite and zinc ferrite. Koop`s, with the help of high dielectric constant, learned high conductivity in ferrites and obtained formula.[8] In 1980, Prof Takieo recommended the use of ferrite material as a power ferrite in the opening international convention of ferrite. Regarding to synthesis and usage of ferrite materials in devices a lot of work is happening in the particular year.

1.3.2 SOFT FERRITES:

Soft ferrites are the kind of ferrites which have low value hysteresis loop and low coercivity value. They can easily be magnetize and demagnetize with and without magnetic field. Material magnetization can easily be reversed without losing much energy. [9]

Following are the properties of ideal soft ferrite

a) Low value coercivity
b) Large value of saturation magnetization
c) Zero value remanence
d) zero hysteresis loss value
e) Large permeability [10]

1.3.3 HARD FERRITES:

Hard ferrites are the kind of ferrites got magnetized when magnetic field is applied and cannot be demagnetized even when magnetic field is removed. They are also known as Ceramic magnetics. Oxides of iron, barium and strontium show the behaviour of hard ferrites. They have large values for hysteresis loop and coercivity also.

1.4 Composition of ferrites:

$\mathbf{M^{+2}Fe_2^{+3}O_4^{-2}}$ is known to be the general chemical formula for ferrites, where M= divalent metal ion for example

- Nickel ion (Ni^{2+})
- Iron ion (Fe^{2+})
- Cobalt ion (Co^{2+})
- Magnesium ion (Mg^{2+})

- Manganese ion (Mn^{2+})

While mixed ferrites are known as combination of different ferrites with equivalent valency. [11]

1.5 Structure of ferrites:

The ferrites having the simplest crystal structure is same as the mineral spinel ($MgAl_2O_4$). It has simple structure contains 32 closely packed oxygen ions in a unit cell.

In spinel structure divalent metal ion M should less than or about 1Å. Most of the divalent metal ions have ionic radius between 0.6 to 1Å which are from spinel family.[12] The crystal with ionic radius of M more than 1Å has poor stability like Ca^{+2} of ionic radius 1.06Å cannot form spinel structure while Mn^{+2} having ionic radius 0.91Å can form spinel structure. In spinel structure there are two types of interstices tetrahedral and octahedral sites. It has total 96 interstices, 72 of them are empty while 24 sites are inhibited by the cations on tetrahedral and octahedral sites. The tetrahedral sites have 8 reserved interstices and each site is surrounded by 4 oxygen ions while the octahedral sites have 16 occupied interstices and each surrounded by oxygen ions.[13]

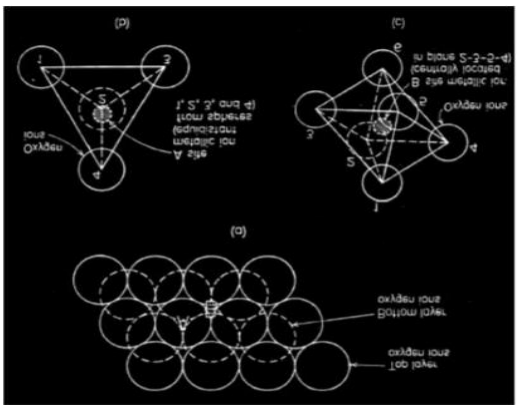

Figure 1.5: Ionic positions (a) Hexagonal Close packing (b) Tetrahedral

(A) site (c) Octahedral (B) site [13]

1.6 Classification of ferrites:

Ferrites are classified in three different groups depend upon their crystal structure.

- Garnet
- Hexagonal
- Spinel

1.6.1 Garnet

$M_3Fe_5O_{12}$ is the chemical formula for garnet ferrites where M represents (yttrium(Y), rare-earth) ions for example Gadolinium, Terbium, Dysprosium and Holmium etc. Silicate mineral and garnets are of same structure. Due to anti-parallel spin alignments along all three sites they have complex net ferrimagnetism. They are magnetically hard ferrites. They have important role in applications of microwave devices.

1.6.2 Hexagonal ferrite:

$MFe_{12}O_{19}$ represents the general formula for hexagonal ferrites whereas M is a diavalent ion. They have extremely complex crystal structure. Their structure consists of oxygen lattice, being FCC contains number of hexagonal coatings of oxygen. This is called hexagonal lattice along additional (vertical) c-axis. Most of hexagonal ferrites got magnetize along this lattice and cannot easily change their magnetization direction towards the other axis. There are three different lattice sites in hexagonal lattice which are surrounded by metal ions

- Tetrahedral site
- Octahedral site
- Trigonal-bi-pyramid

While each side of metal ion is occupied by six oxygen ions.

1.6.3 Spinel ferrite:

Spinel ferrites are the ferrites that are cubic in structure and are known as soft ferrites which can easily change their magnetization direction by applying external field. Their properties are highly dependent upon the arrangement of metal ions (divalent/trivalent) on both sites. On different cationic distribution they are categorized differently. [14]

- Normal spinel
- Inverse spinel
- Random spinel

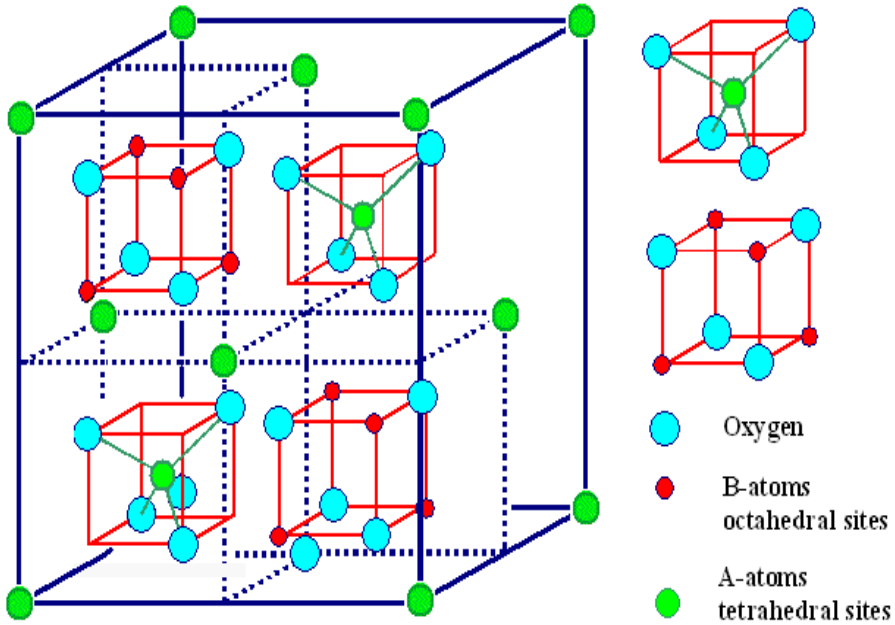

AB_2O_4 spinel The red cubes are also contained in the back half of the unit cell

Fig 1.6 Unit cell of spinel ferrite[15]

1.6.3.1 Normal spinel ferrites:

In normal spinel ferrite composition, octahedral sites (B) and tetrahedral sites (A) are inhabited by trivalent metal ions and divalent metal ions respectively. In these spinel ferrites structure there are no A-B interactions as A site metal ions are non-magnetic while B-B interaction exists in which half of the magnetic ions lines up in one direction and half non-magnetic in other direction. $MgAl_2O_4$ and $FeCr_2O_4$ are known as normal spinel ferrites. $\mathbf{(M^{2+})A\ (Fe^{+3})B\ O_4^{2-}}$ is the cationic distribution for normal spinel ferrite, where M is divalent metal ion.

1.6.3.2 Inverse spinel ferrites:

As compare to normal spinel ferrite structure, in inverse spinel ferrite tetrahedral site (A) is occupied by one trivalent ion (Fe^{+3}) while the octahedral site (B) is occupied by remaining Fe^{+3} and M^{+2}. They are known to be simplest ferrites and

$CoFe_2O_4$, $MnFe_2O_4$ and $NiFe_2O_4$ are the common examples. $\mathbf{(Fe^{+3})A\ (M^{+2}\ Fe^{+3})B\ O_4^{-2}}$ is the cationic distribution for inverse spinel ferrite, where M is divalent metal ion.

1.6.3.3 Random spinel ferrites:

In mixed spinel ferrites the trivalent metal ions and divalent metal ions are allocated randomly at both tetrahedral and octahedral sites that's why they are called random spinel ferrites. $CuFe_2O_4$ is an example of random spinel ferrite. The distribution of metal ions on both sites depends on the synthesis and sintering process.

$\mathbf{(M_\delta^{2+}Fe_{1-\delta}^{3+})A\ (M_{1-\delta}^{2+}Fe_{1+\delta}^{3+})\ B\ O_4^{2-}}$ is the cationic distribution for random spinel ferrites. [16]

1.7 Dielectric Properties:

Ferrites have high activation energy which indicates their high resistivity at room temperature. This property of ferrites makes them suitable for applications as dielectric materials. The non-conducting materials are mainly used as dielectric materials it is very informative to study the interaction of electric field with the atoms of dielectric materials. In dielectric materials polarization occurs when they are exposed to an electric field, the polarization results due to the occurrence of induced dipole moments. When a field is applied the electron, cloud move to one side resulting in the creation of dipoles which is characterized by its dipole moments [20]. In dielectric material each atom creates its small field, and this field interact with the field which is applied from the outside [21].

The electric polarization is referred to interfacial or space-charge polarization as it is linked with the charges that are either trapped or mobile. This type of polarization mainly occurs in the amorphous and polycrystalline materials because in such type of material charge carrier like electrons, holes and ions are trapped on some sites and they get mobilize after getting some energy [23] . The mechanism which is responsible for the transportation is defined by knowing the dielectric behavior of a dielectric material depends upon of a dielectric material is its dielectric material depends upon which generally defines dielectric material depends upon a dielectric material. The dielectric constant of a dielectric material depends upon the different factors. The dielectric constant and the dielectric polarization field both depends on

each other. The dielectric polarization fluctuates accordingly to the fluctuation of external field. If fluctuations of polarization do not complement the fluctuations of external field then the dielectric of that material decreases [24]. In case of low frequency applied fields, the polarization follows the fluctuations of the field and hence in that case the dielectric constant remains same. In case of high frequency applied fields, the polarization is not able to follow field and its dielectric constant decreases and at one stage when the frequency to very high value then the orientation polarization stops due to relaxation of dielectric materials [25]. There are different limits of frequencies at which the different types of polarization (ionic, electronic etc.) stop.

1.8 Nano Science

NANO is the science of today, it tightens it grip on all over the world. It consists of several disciplines of science like, Physics, Chemistry, Biology, material science etc. It has a lot of applications which are available in markets now days. Nanomaterials have totally different properties than bulk materials. The physical properties of a substance changes as we move from its bulk form to its Nano form. We can define Nano-materials as, those materials which have structured components with at least one dimension less than 100 nm. On the basis of dimension structure, the Nanomaterial are categorized as 1-D, 2-D and 3-D. 1-D are those Nanomaterials whose one dimension is constrained only, examples of 1-D Nanomaterials are thin films and surface coatings [26]. Its sizes can be varying in 2-dimensions, while its 3rd dimension will always have constrained less than 100nm. Similarly, in case of 2-D and 3-D Nanomaterials 2 and 3 dimensions will remain less than 100nm in its Nanoscale materials. For example, Nanotubes and Nanowires are 2-D Nanoscale materials in which two dimensions are always remain in the range of Nanoscale. Precipitates, collides and quantum dots are the examples of 3-D nanostructures. In case of these particles, all the three dimensions are constrained to nanoscale. Which means that all the three dimensions of a 3-D nanostructured material remain less than 100 nm.

As the nanomaterials have different properties than its bulk counterpart. The main reasons which are responsible for their changes in properties on nanoscale are relatively large surface area and quantum effect [26]. These two reasons or properties of a material are responsible for the change of different material properties like

electrical properties, strength and their reactivity. As we move from bulk to nanoscale, surface to volume ratio of a material increases which in the result enhances different properties like electrical properties and magnetic properties [27].

In nanotechnology or Science, a new material is fabricated rather by handling different and new techniques (like a vast variety of techniques used for the fabrication of thin films) or in the result of self-assembly. Nanotechnology has already been given us a lot of new materials and new methods in almost all fields of science and yet more to be discovered. Those materials are very important and useful in those fields.

1.9 DC electric properties:

There are three basic types of materials which are conductors (metals), insulators and semiconductors. They are categorized on the basis of their tendency to carry electric charge. The materials which are good carrier of electric charges i.e. having higher conductivity have the lower activation energy. The insulators have very high activation energy. In case of some insulators and semiconductors their conductivity increases by increasing temperature but in case of metal a gradual decrease occurs in the conductivity of metals as we increase the temperature. Ferrites are structure sensitive materials the conduction of electric charges in the ferrites depends upon the structure of the ferrites. The structure of ferrites can be changed by its synthesis route, amount of substituents, annealing temperature, reaction temperature, type of substituents etc. [28] As compared to metals, ferrites have high electrical resistance and its electrical resistivity can be controlled or enhanced by the controlling the factors defined above [29].

By the electrical properties of a materials depends on the generation of the electric charges in the material and their transport inside the material. In ferrites the conduction or transport of charge carriers occur in the form of hopping which is explained in the Verwey model [20]. The hoping of charge carriers in the ferrites occur between the ions at sites octahedral. The jumping on the separation from one to other the ions, for the conduction of charge in ferrites the charge carries must have overcome the potential barriers i.e. the charge carrier should have much energy to hope from one ion to another. That minimum energy which charge carrier required to overcome the potential barriers is known as activation energy [21]. The

transportation of charge carriers in M-type ferrite materials is also occurred by hopping thus they are hopping semiconductors or it is said to be small polar an hopping semiconductors having large number of mobile electrons [22]. The exchange of electrons ferrites occurs among the ferric and ferous ions which are situated on octahedral sites [21]. This exchange can be different in different materials depending upon the orbital overlapping of Fe^{3+} and Fe^{2+} with oxygen [23]

1.10 Applications of ferrites:

Ferrites play an important role in different fields. Now days scientists are interested in ferrites doping. Which can be prepared by different composition, synthesis techniques and with various cationic concentrations which in result effects the properties of ferrites like electrical, magnetic and dielectric properties. Ferrites have specific magnetic properties and have applications in power conditioning, electromagnetic device, electromagnetic wave absorbers, magnetic inks for bank cards, and recording media etc. Following are the some important fields of ferrites

- Medical diagnostics and treatments
- Drug delivery
- Magnetic shielding
- Magnetic sensors
- Electromagnetic interference suppression
- Pollution control
- High frequency applications [2]

1.11 Objectives of this research:

The objective of this research is

- Synthesis of $CoFe_2O_4$, CoMgFe2O4, $CoMnFe_2O_4$, $CoZnFe_2O_4$ and $CoNiFe_2O_4$ nanoparticles through sol gel synthesis technique.
- Material Characterization using XRD, FTIR, EDX and SEM.
- Study of dopant effect on dielectric and magnetic properties.

(Chapter 2)

Theoretical review

2.1 LITERATURE REVIEW:

Material	Method	Characterization techniques	Properties	Application	Reference
$CoCl_2.6H_2O$, $ZnCl_2$, $FeCl_3$, SDS, NaOH, H_2SO_4 , H_2O_2, Rhodamine B, ethanol , n-butanol, C_6H_{14}	Reverse micelle method	XRD, FTIR, HR-TEM and VSM	Saturation magnetization decreases with increasing Zn^{2+} concentration, showed increased in degradation with increase in Zn^{2+} ion doping.	Photocatalysis	[30]
Cobalt nitrate, magnesium nitrate, ferric nitrate, L-arginine, rhodamine B, hydrogen peroxide and hydrochloric acid, distilled water was used as solvent	Simple microwave combustion method.	XRD,SEM,FTIR,VSM and EDX	The efficiency value of photodegradation was observed 99.5 % at concentration of 0.4 that was highest efficiency of all	Photocatalysis	[31]
Fe(NO3)3 9H2O, Co(NO3)2 6H2O, Holmium	Reverse micelle technique.		The maximum efficiency (99%) of degradation was found to be for $NiFe_2O_4$ in 20	Photocatalysis	[32]

nitrate $Pr(NO_3)_3 6H_2O$, $Sm(NO_3)_3 6H_2O$, $Tb(NO_3)_3 6H_2O$, sodium borohydride $NaBH_4$ are used as raw materials.			min as catalyst		
$Fe(NO_3)_3.9H_2O$, $Co(NO_3)_2.3H_2O$, ruthenium (III) chloride hydrate, citric acid, hydrogen peroxide, Ethylene glycol, Remazol Deep red dye	sol-gel method	XRD, SEM, EDX and TEM. UV visible reflectance spectroscopy for optical analysis.	$CoRu_{0.06}Fe_{1.94}O_4$ showed the maximum results for the photocatalytic degradation of remazol deep red.	Photocatalysis	[33]
cobalt nitrate, iron nitrate, lanthanum nitrate, sodium hydroxide, NaOH, P.V.A	Co-precipitation technique	XRD, impedance analyzer and VSM	The dielectric and magnetic loss is quite low for prepared ferrites. With an increase in La^{3+} ion concentration saturation magnetization decreases		[34]
$Co(NO_3)_2 6H_2O$,	Sol gel combustio	XRD, FTIR, VSM and TEM	The saturation magnetization	Photocatalysis	[35]

Cr(NO3)39H2O, citric acid, Zn(NO3)26H2O	n method		showed maximum value at x=0.4. With the increase in concentration of copper the photo catalytic degradation of MO dye increases		
$Zn(NO_3)_2$ • $6H_2O$, $Co(NO_3)_2$ •$6H_2O$, ferric nitrate, Congo red (CR) dye.	Combustion Method	XRD, SEM with EDAX, TEM, FTIR	The maximum values for the degradation of Congo red and Evans blue were achieved for $Zn_{0.4}Co_{0.6}Fe_2O_4$ when compared to $CoFe_2O_4$	Potocatalysis	[36]
Bismuth Nitrate, Manganese Nitrate, Citric acid, Nitric acid.	citrate precursor method	XRD,FESEM, FTIR and VSM	With the increase in doping concentration the value of dielectric constant was found to be increased. The maximum value of coercivity and saturation magnetization was obtained at x=0.05 and x=0.075		[37]
$Co(NO_3)_2$· $6H_2O$, $Zn(NO_3)_2$· $6H_2O$ and NaOH as a precipitant.	Co-precipitation method	XRD,EDS,FTIR , DRS and VSM	By increasing dopant concentration saturation magnetization increases from 5.7		[38]

			to 80 emu/g respectively. Band gap decreases with increasing dopant.		
cobalt nitrate, $Pr(NO_3)_3 \cdot 6H_2O$, Samarium nitrate, Holmium nitrate, $Tb(NO_3)_3 \cdot 6H_2O$.	hydrothermal method	XRD, SEM, TEM, VSM and Dielectric properties.	Due to doping of rare-earth dopant to cobalt ferrite decrease the coercive force, saturation magnetization, the ratio of remanence to saturation magnetization (MR/MS)		[39]
Zinc nitrate, nickel nitrate, ferric nitrate,	Microwave combustion technique	XRD, FTIR,HR-SEM,EDX,HR-TEM,DRS and VSM	Saturation magnetization value increased with increasing Ni content. Photocatalytic activity enhanced with increasing Ni content		[40]
$FeCl_3.6H_2O$, $NiCl_2.6H_2O$, $MgCl_2$,	Co-precipitation method	XRD, FTIR, FE-SEM,EDX, VSM and Dielectric Properties.	Saturation magnetization and magnetic moment decreases while coericitivity increases. The dielectric analysis showed higher value of dielectric constant for low		[41]

			frequency range		
$Co(NO_3)_2$, $Fe(NO_3)_3$, $Yb(NO_3)_3$ and NH_3	Co-precipitation method	XRD, Dielectric properties, VSM	dielectric loss decreased while AC conductivity increases with increasing content Saturation Magnetization was decreased while coercivity increased		[42]
bismuth nitrate pentahydrate, yttrium nitrate hexahydrate, iron nitrate nonahydrate	Facile green route	XRD, HRTEM, FESEM, DRS and VSM	bandgap energy decreases from 2.07 to 2.05 eV. photodegradation efficiency was enhanced.	photocatalysis	[43]
Cobalt nitrate, magnesium nitrate, urea as a fuel, ferric nitrate	sol-gel combustion method	XRD, HR-SEM, HR-TEM, EDX, FTIR, VSM	From VSM results it was concluded that both saturation magnetization and coercivity increased	Photo Catalytic Degradation	[44]

(Chapter 3)

Experimental and characterization techniques

3.1 Experimental techniques:

Nanoparticles are synthesized in two processes

1. Top-down approach
2. Bottom-up approach

A process of transforming large structures into fine and small structures using different methods for example ball milling, lithography, laser ablation, electro spinning, arc discharge etc. while bottom-up approach is a process in which atoms, molecules and clusters are combined to form nanoparticles structures. Bottom-up approaches includes wet chemical synthesis, CVD, PVD, MBE, self-assembly, hydrothermal synthesis etc.

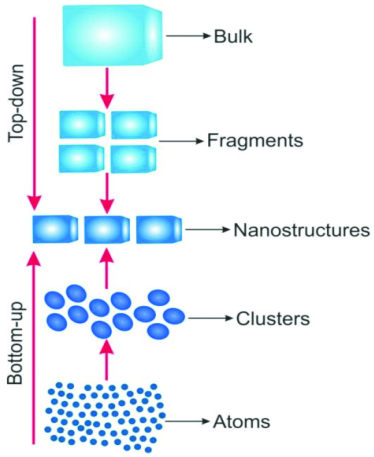

Fig 3.1 Top-down and Bottom-up approach[71]

Each technique has several advantages and disadvantages. There are some advantages and disadvantages of both top-down and bottom-up approach. It is

difficult to attain homogeneity and smaller size nanoparticles with high purity in top-down approach. While bottom-up approach is expensive as compare to top-down approach.[2]

Ferrites are synthesized using different methods as shown in fig 3.2

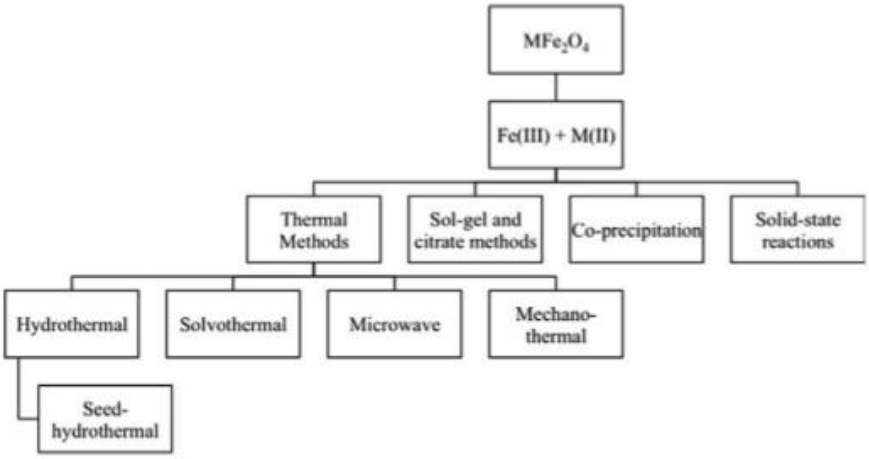

Fig 3.2 Synthesis techniques of ferrites using Fe(III) and M(II) salts as precursors

3.1.1 Solid state reaction method:

This method is mostly used for the preparation of ceramic materials due to its simplicity. In solid state reaction method, final products are formed by the direct reaction of solids without any decomposition. For maximum contact between the reactants, they should have large surface area. At low temperature solids do not react with solids so high temperature is required for higher rate of diffusion. Structural similarity between reactants and products lead to increase in rate of nucleation.[45,46] Following are the main points for conventional solid state method

- The selection of accurate precursor material.
- From the stoichiometric calculations weigh the accurate ratio of starting material.
- Mixing of reactants using agate motor and pestle or ball mill.
- Then the product is heat treated at certain temperature to get the required phase.

- Finally, the obtained product is grinded to get the fine particles.

The main advantages of this method are simplicity, cheap starting materials and clean reactions. While the major disadvantages are poor homogeneity distribution for dopants, high calcination temperature, uncontrollable particle size and low surface area.[47] To overcome these issues wet chemical methods are introduced.

3.1.2 Wet Chemical techniques:

The main importance of wet chemical techniques is homogeneous mixing of precursors and controllable particle size, attainable surface morphology and surface area. It's some major advantages are lower calcination temperatures, low impurity phases and high surface area. Following are some main wet chemical techniques

- Co-precipitation
- Sol-gel
- Hydrothermal etc.[47]

3.1.2.1 Co-precipitation:

The co-precipitation technique includes nucleation, growth coarsening and agglomeration, all of these processes happens simultaneously.

The co-precipitation process consists of following points: [48]

- Metal preparation using aqueous medium.
- Removal from non-aqueous medium.
- Using both aqueous and non-aqueous medium for oxide synthesis.
- Decomposition of metalorganic raw material.
- Reduction of electrochemical reactions.
- Co-precipitation through microwave or sonication assisted.

Some important properties of co-precipitation method:

- The final products formed at high degree of supersaturation are insoluble species.
- Nucleation is one of the main step in which large number of tiny particles are formed.
- Properties of final product are highly dependent of secondary processes e.g Ostwald ripening and aggregation.
- Supersaturation conditions are compulsory for precipitation to occur. Given reaction lead to these conditions

$$xA^{y+}(aq) + yB^{x+}(aq) \longleftrightarrow A_xB_y$$

3.1.2.2 Sol-gel Method:

Sol-gel is a process of inorganic polymerization. In 1864, it was firstly introduced by Ebelmann. [50]. It is a process of gel formation by the combination of sol. Sol can be in the form of a solution. Sol is basically a colloidal particles which leads to the formation of Nanoparticles. In sol gel process, metal alkoxide and metal chlorides are the mostly used precursors. Sol is formed when precursors go through polycondensation and hydrolysis reactions. Sol is effectively a structure of completely dispersed nanoparticles in a solvent. Inorganic continuous network is obtained of liquid phase known as gel.[49] To remove the liquid phase the gel is then dried. Then the dried sample is calcined at required temperature to enhance the mechanical properties and favour more polycondensation reaction.

There is another method known as sol gel and citrate method. In this technique, along with metal and iron salts critic acid is added into the solvent. To maintain the pH at 9 sodium hydroxide is added periodically. In the result, the obtained gel is then dried and heat treated at 600 ºC.

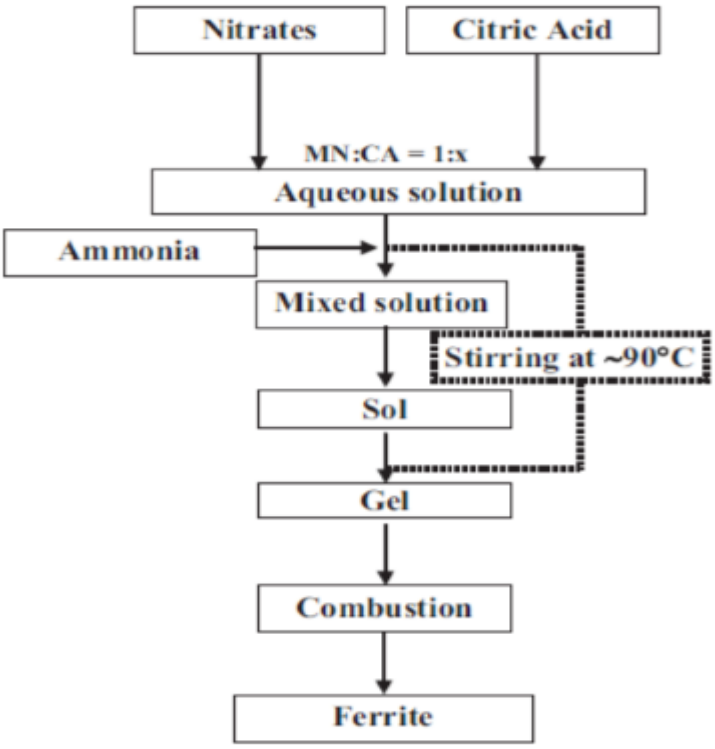

Fig 3.3 flow chart of sol-gel combustion method

Factors affecting Sol-gel synthesis:

There are many factors that can effect the properties of a sample during the sol gel synthesis process like electrical, mechanical, magnetic, morphological, particle size etc.

Some of main factors are given below

- Effect of chelating agent
- Effect of pH

Effect of chelating agent: Precursors and chelating agent utilized for synthesis of ferrite nanoparticles with the ratio 1:3. The properties of nanoparticles can highly affect ratio and type of chelating agent. Chelating agent commonly used are urea, citric acid, glycine, hexamethylenetetramine etc.[51] Each chelating agent acts differently during combustion like combustion process for hexamethylenetetramine and glycine occurs within few seconds while for citric acid and tartaric acid it took more than 30 minutes and for urea it took 2-3 minutes. [52]

Effect of pH: In sol gel process ammonia is used to maintain the value of pH. It

Effects the condensation and hydrolysis reaction. Combustion rate depends on pH

Value.[53] Small size nanoparticles are obtained for pH in the range of 7-8 due to fast gelation. While pH between 2-3 results in extended network due to slow gelation.

In our research work Sol-gel method was employed successfully for preparation of ferrite nano particles by given formula $Co_{1-x}M_xFe_2O_4$. Pure and doped sample were prepared by taking a fix concentration of the Ni, Zn, Mg and Mn as given here

I. $CoFe_2O_4$
II. $Co_{0.5}Ni_{0.5}Fe_2O_4$
III. $Co_{0.5}Zn_{0.5}Fe_2O_4$
IV. $Co_{0.5}Mg_{0.5}Fe_2O_4$
V. $Co_{0.5}Mn_{0.5}Fe_2O_4$

3.2 Characterization techniques:

3.2.1 X-ray diffraction (XRD):

X rays are the radiations known as electromagnetic radiations having wavelength of 1Å. In electromagnetic spectrum it has shorter wavelength than UV while longer than gamma rays. They are commonly used to measure atom's phase and structural arrangement. X-rays are produced when solid target like copper or molybdenum is attacked by high energy charged electron beam accelerated using high voltage field. The inner shell electrons of the targeted atoms are ejected by the high energy electron bombardment by ionization process. The vacancy left is then filled by the free electron which results in emission of radiations. Energy is given as

$$E = \frac{hc}{\lambda} \qquad (1)$$

Where "h" and "c" in the equation are known as plank's constant and speed of light in vacuum.

These X-rays strike the crystal and some of them are deflected after collision, these deflected X-rays gives information about the electron distribution in the material. While each crystal has its own deflection pattern which can be used as its 'fingerprint'.

Bragg's law describes the simple description for X-ray diffraction from crystal. Fig 3.3 shows the Bragg's law details.

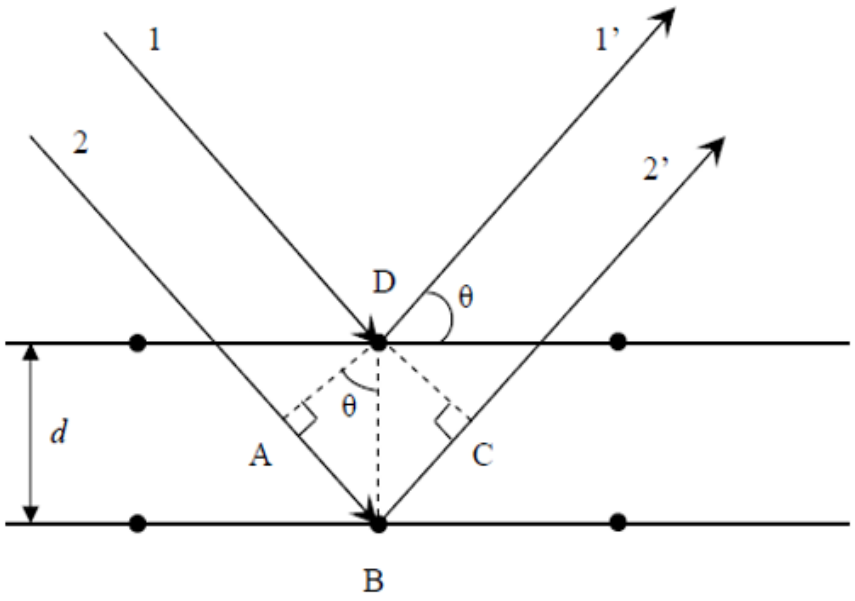

Fig 3.4 Description of Braggs Law[1]

From the fig the incident ray 1 and 2 are in phase and parallel to each other upto the points A and D, the ray 1 strikes the upper surface at point D of the atom, while the ray 2 strikes the lower surface at point B of the atom covering the extra distance, as compare to ray 1, of AB+BC and become parallel again as ray 1 and 2.

In fig d is given as the vertical distance and angle of incidence is denoted by θ. So

$$AB = BC = d \sin \theta$$

$$2AB = n\lambda$$

$$\mathbf{2dsin\theta = n\lambda} \quad \mathbf{(2)}$$

The crystal unit cell parameter can be found by d spacing (distance between adjacent atomic planes d). While for cubic crystal

$$\alpha = \beta = \gamma = 90^{o}$$

so d-spacing is given as

$$1/d^2_{hkl} = h^2/a^2 + k^2/b^2 + l^2/c^2$$

Whereas hkl are known as miller indices and a, b, c are unit cell parameters.

If crystal is cubic so a=b=c, the equation is given as

$$1/d^2_{hkl} = h^2+k^2+l^2/\ a^2$$

Powder x-ray diffraction is a characterization technique which uses Debye-Scherrer formula to calculate the material crystallizes size. The Debye-Scherrer equation is given as

$$D_{XRD} = 0.9\lambda/\beta cos\theta$$

Peaks having significant intensities were analysed for calculations.

3.2.2 Scanning electron microscopy (SEM):

Scanning electron microscopy is a characterization tool in which focused electron stream generated by tungsten filament mounted electron gun for the thermionic electron emission to illuminate sample for images. The electron beam before got incident onto the sample were focused to a spot with ~4-50 Aº diameter using condenser lenses and controlled with the help of deflection coil. When electrons hit the sample the electron loses their energy by converting it to different types of energies like heat energy, ejection of secondary electrons, X-rays or light emission which are detected by specialized detectors.

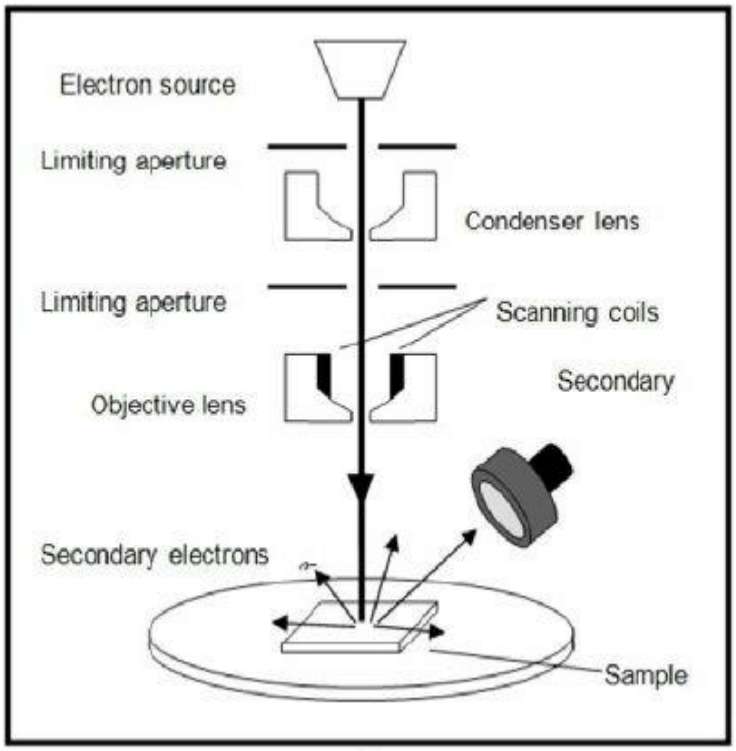

Fig 3.5 Schematic diagram of SEM [72]

The main steps for the sample preparation are given as

- Sectioning
- Mounting
- Grinding
- Polishing
- Etching [54,55]

3.2.3 Fourier Transform Infrared spectroscopy (FTIR):

In electromagnetic spectrum, Infrared radiation lies between microwave and visible region. The wavelength of Infrared radiation is smaller than microwaves and longer than visible radiation while frequency is higher than microwave and smaller than visible light. The infrared region is divided into three regions

- Near IR (closer to visible)
- Mid IR(between visible and microwave)
- Far IR(closer to microwave)

The IR radiation is produced thermally by the motion of atoms and molecules in the sample. The higher the temperature leads to increase in movement of atom results in more IR radiations. [56]

FTIR is a characterization technique that uses a light which is absorbed by the sample at certain wavelength. This technique is used to measure the photoconductivity, Raman scattering, emission spectra's and absorption. Chemical purity and stretching modes of the material can be measured using FTIR spectroscopy. The data is collected by the spectrum of matter.

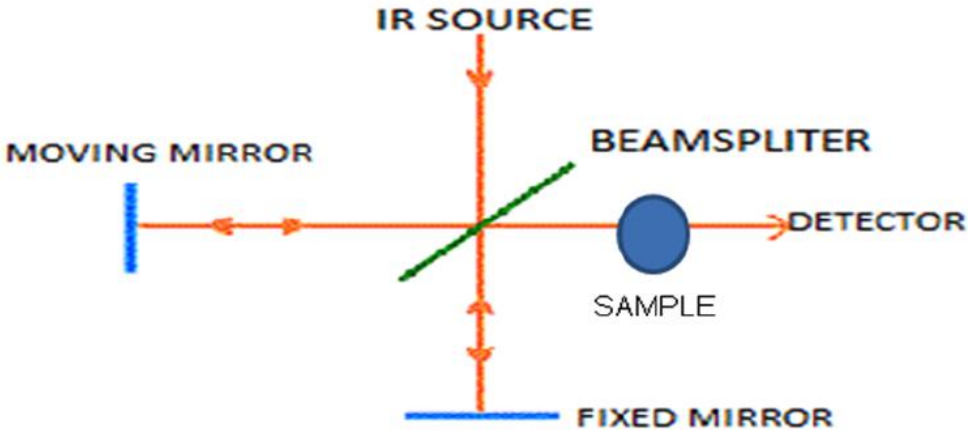

Fig 3.6 Schematic diagram for FTIR [73]

In FTIR, a polychromatic source of an infrared light is made to strike the splitters. Incident light is half refracted towards fixed mirror while half transmitted through moving mirror which passed through the material. From the interaction of light with sample the molecular component and sample structure can be obtained.[57]

When applied IR frequency is equal to natural frequency of vibration the radiation is absorbed and results molecular vibration. So different bond or functional groups required specific frequency for absorption which results in a specific characteristic peak for every functional group. This technique is used for the determination of different organic compounds.[56]

Applications:

1. Liquid chromatography fraction analysis.
2. Infrared microscope is used to check very small samples.[57]

3.2.4 Energy dispersive spectroscopy (EDS):

EDS is used to study the chemical properties of the material and is always used in conjunction with Sem or Tem. The working principle of EDS is defined as the bombardment of focused high energy electron beam onto solid specimen which results in generation of X-rays. Further detectors in make use these generated X-rays for chemical analysis with the resolution of 150 eV. EDS technique can also be used for Quantitative analysis and elemental mapping.

When solid sample is bombarded by the high energy electron, the electrons in the atomic shell of sample are ejected and leaving behind the vacant space. This is further filled by the electrons from higher energy levels and leads to generation of X-rays. These emitted radiations have characteristics energy values. Elemental analysis from EDS becomes possible because of the certain energy value each element have in periodic table.

When the L-shell vacancy is filled by the K-shell electron Kα X-rays are emitted. Letters K,L,M are known as the shells that emit electrons while α,β,γ are the shells where these electrons are substituted. In periodic table from beryllium to uranium (atomic number 4to 92) all the elements can be analysed by EDS.[58,59]

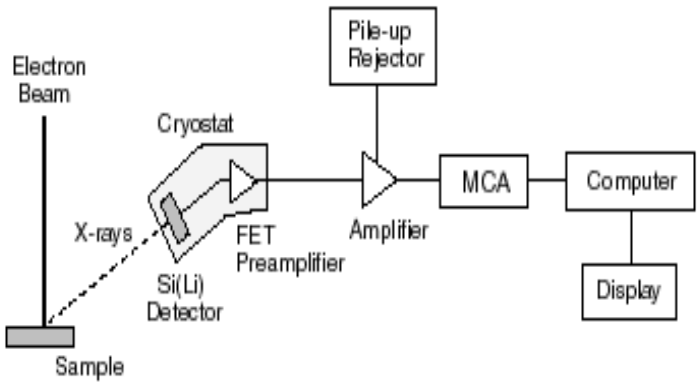

Fig 3.7 Schematic diagram of EDX[74]

3.2.5 Ultraviolet/visible spectroscopy:

UV visible spectrometer is a device through which absorbance of visible or ultraviolet light by a specimen can be studied. As it is known that visible light contains a spectrum of electromagnetic radiation having both electric and magnetic portions. However UV visible spectroscopy only deals with electric portion that's why also known as electronic spectroscopy. The main purpose of this

procedure is absorption of certain energy quantity which results in the transitions from lower energy to higher energy levels. UV region lies in the range of 190 nm to 400 nm while visible lies within 400nm to 800 nm area. The short UV spectroscopy works in the range of 200 nm-800 nm and transition in energy level occurs when absorption of light occurs in this range.

There are various transitions due to absorption of light happens between HOMO to LOMO. Lowest energy orbitals corresponds to s-orbital denoted by sigma (σ) bonds while higher energy orbitals relates to p-orbital denoted by pie (π) bonds. Non-bonding orbitals are higher energy levels as compare to p-orbital while an tibonding pie (π^*) and sigma (σ^*) are the highest. Transitions due to light absorbance are shown in fig 3.7

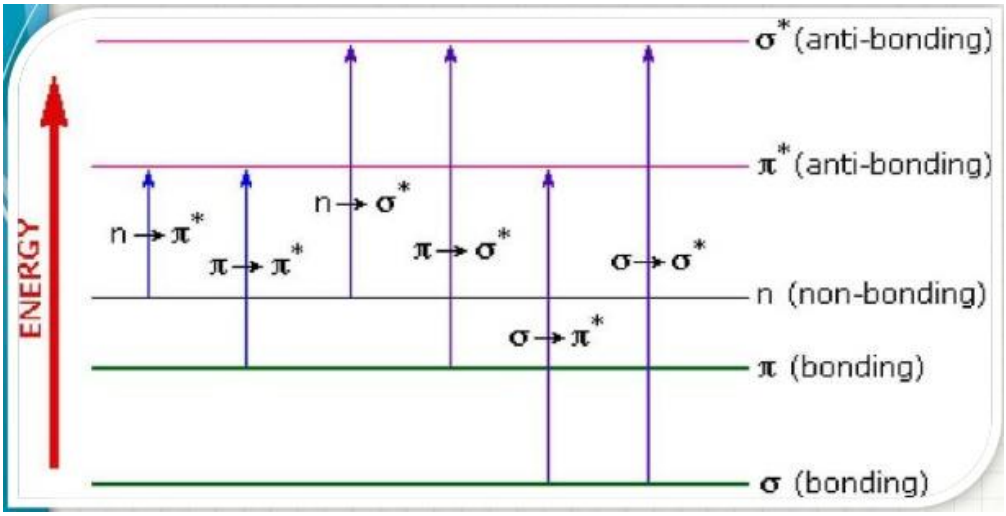

Fig 3.8 Electronic transition spectrum [75]

Construction and working principle:

To cover the whole UV and visible range the source is made up of tungsten, halogen and deuterium lamps. Tungsten generates the rays having wavelength >375 nm while halogen and deuterium covers the range <375 nm. It contains a monochromator having slits and prism. These rotating Prism are used to scatter radiations while slits separates single beams which are monochromatic and with the help of another prism these beams are further divided into two more beams. One of

these two beams is passed from refrence solution while the other beam through sample solution. A cell contains both the solutions made up of quartz and silica. While two detectors are used having photocells. Beams from sample cell and reference cell are received by these two detectors. The beam generated by sample cell is stronger and alternating current in photocell is produced. While amplifier next to detector is used to enhance the signals received. While in the end a pen recorder is installed parallel to amplifier directly connected to computer that is used to store data and spectrum depiction.

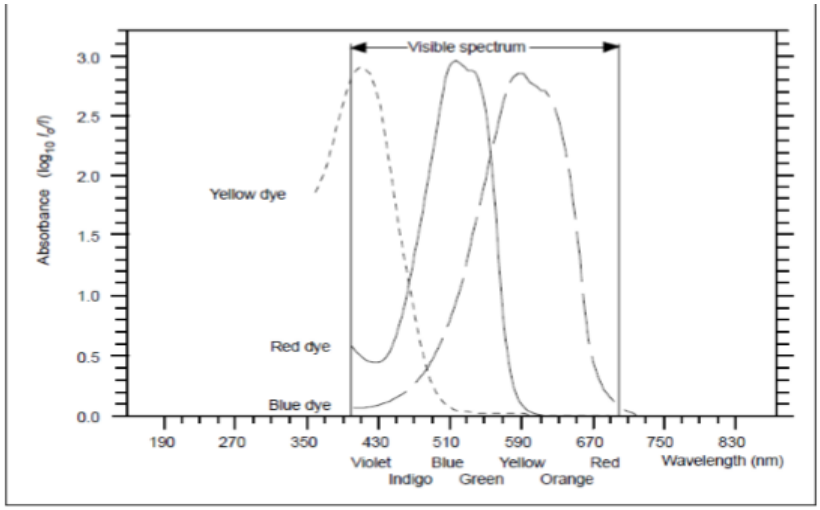

Fig 3.9 Absorption of light by dyes

From Beer's law, the absorption depends upon the absorbing molecules (for dilute solutions only). While from lambert's law, radiations which are absorbed are independent of their intensity. From these two laws beer-lambert law is introduced

$$Log_{10} \frac{I}{I_o} = \varepsilon lc$$

Where I_o, I, ε, l and c represents the radiation intensity, transmitted radiation intensity, molar absorption coefficient, absorbing solution path length and absorbing molecules concentration.

The value for $\log_{10} (I_o/I)$ represents the solution absorbance which can be directly studied from the spectrum. Absorption constant called as molar absorption coefficient doesnot depend upon concentration and path length while absorption is dependent of both the concentration and path length.

While another important information can be calculated from λ_{max}, which is the maximum absorption at certain wavelength. If ε and λ_{max} are known Solution concentration can be calculated, while both the terms depends on solution nature. [61]

3.2.6 Electric properties:

3.2.6.1 Dielectric Properties:

The dielectric properties such as dielectric loss, dielectric constant can be found using LCR Meter Bridge. Formula for Dielectric constant

$$\varepsilon' = \frac{Cd}{A\xi_{\circ}}$$

Whereas C represents capacitance, while *d*, *A* and ξ represents the pellet thickness, area and permittivity constant.

Energy dissipation losses can be calculated by

$$\varepsilon'' = \varepsilon' * D$$

Dielectric materials have some power losses due to work done to resist damping and frictional forces. Dielectric tangent loss can be found by

$$tan\ \delta = D = \frac{\varepsilon'}{\varepsilon''}$$

For AC conductivity given equation is used:

$$\sigma_{ac} = \omega\varepsilon\xi_{\circ} tan\delta$$

3.2.6.2 AC impedance spectroscopy:

AC impedance measurements are calculated at room temperature. Reactance (X) and Resistance (R) is found in between the frequency of 100 Hz to 5 MHz. Impendence can be calculated from given relation

$$Z = R + jX$$

Where R and X shows the real and imaginary parts of impedance. Material resistivity is represented by impedance-cole plot and 'Ω' is its IS unit. While resistance (R) and Reactance (X) are represented as impedance real and imaginary parts

$$Z' = R = |Z| cos\theta z$$

$$Z'' = X = |Z| sin\theta z$$

3.2.7 Vibrating sample magnetometer (VSM):

In 1959 simon foner in lincolan laboratories created first vibrating magnetometer sample. It is used to study magnetic properties at different temperatures for every kind magnetic materials like ferromagnetic, antiferromagnetic, diamagnetic, paramagnetic and ferromagnetic.

Principle: faraday's law of induction is the basic principle on which VSM works. In which sample is vibrated at a fixed amplitude with a homogenous magnetic field. It contains pick up coil which is stationary with respect to vibrating sample. Voltage is generated with the change in applied magnetic field in pick up coils.

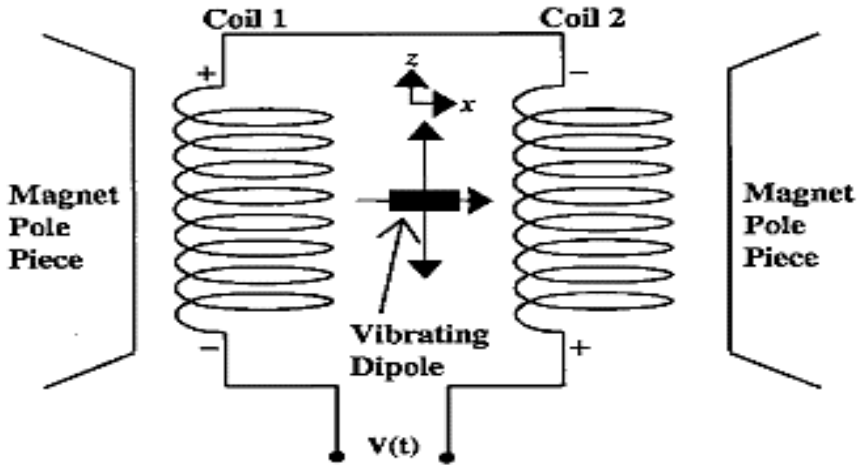

3.10 Principle of Vibrating Sample Magnetometer[63]

3.2.7.1 Parts of VSM:

- VSM contains water cooled electromagnet along with power supply which is used to magnetize the material.
- Sample holder and Vibration exciter is made up of sample rod used for sample holding between pick up coil pole pieces and Material holder is further attached to vibration exciter used to vibrate the

sample at fixed frequency. By rotating the sample holder to expose the material at different angles to constant magnetic field. Chassis is used to control vibration exciter oscillation.

- It has sensor coils in which alternating current is generated when sample is vibrated at a fixed frequency. Further signals generated are amplified by amplifier attached for sample magnetization confirmation .
- Lock-in-amplifier is used for signal amplifier by removal of noise and only takes signal generated by vibrating sample.
- Computer interface is used for data collection. [62]

(Chapter 4)

Results and Discussion

4.1 XRD ANALYSIS:

The pattern for XRD of $CoFe_2O_4$ nanoparticles (fig 4.1) confirms the cubic spinel structure. The diffraction peaks at 2θ values of 29.9°, 35.28°, 37°, 43.04°, 53.36°, 56.88° and 62.48° are allotted to (220), (311), (222), (400), (422), (511) and (440) planes respectively.

The diffraction peaks are matched well with JCPDS Card no. 22-1086.

There is no extra peak found in the pattern resulting in single phase cubic structure

4.1.1 $CoFe_2O_4$ doped with Ni,Zn,Mg, Mn($Co_xM_xFe_2O_4$) :

Through sol-gel method Cobalt ferrite was doped with the concentration of x= 0.5 .XRD measurements were done of samples after annealing of 3hr at 800 degrees. The miller indices h,k,l values for doped samples matches with the Cobalt ferrite with JCPDS card no. 22-1086.

There is no separate peak found after the doping of metallic cations Ni, Zn, Mg and Mn because of minimalistic difference in ionic radii of Co^{2+} and the doping elements. The ionic radii of Co^{2+} is 0.76 A^o while the ionic radii of Ni^{+2}, Zn^{2+}, Mg^{2+} and Mn^{+2} is 0.69 A^o,0.82 A^o, 0.72 A^o, 0.83A^o respectively. So the ionic radii of cobalt and dopants are comparable resulting replacement of cobalt by cations at both sites.

The following relation was used to calculate the lattice parameters of pure and doped samples.

$$\frac{1}{d^2} = \left(\frac{h^2+k^2+l2}{a^2}\right) \quad \text{..... (5.1)}$$

Where a represent the lattice parameter as for cubic structure a=b=c. h, k, and l are the miller indices of identified peaks while the d represents the d-spacing between two lattice planes.

With the addition of metallic cations as the dopant in cobalt ferrite, a slight change in lattice parameters was observed, probably because of minute change in ionic radii of cobalt and metallic cations.

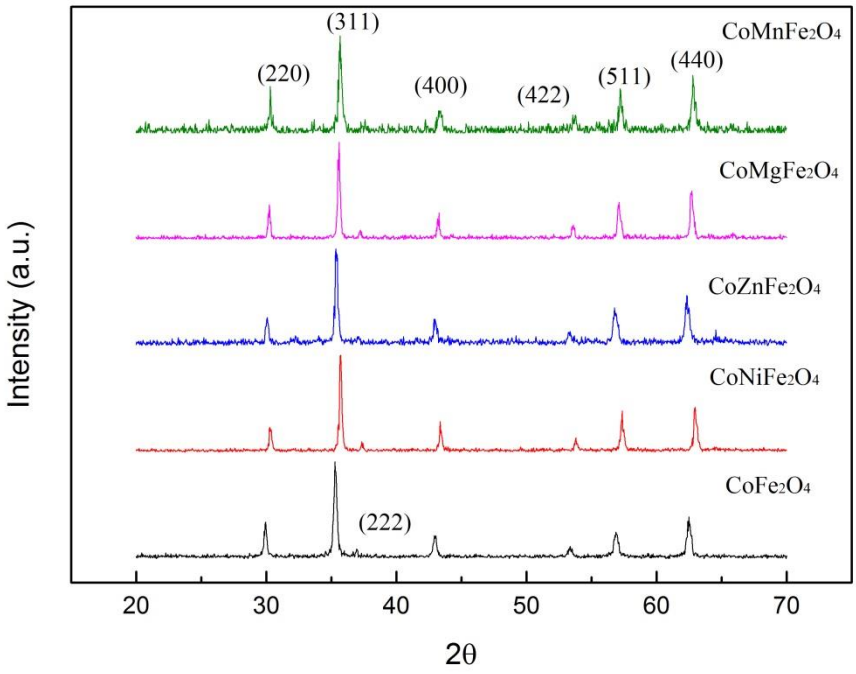

Fig 4.1 XRD pattern for Pure and doped Cobalt Ferrite Nanoparticles

Table 4.1: Lattice parameter and crystallize size of prepared samples

Sr. No.	**Prepared Sample**	**Lattice parameter**	**Crystallite Size**
		a (Å)	
1	$CoFe_2O_4$	8.58	38.7nm
2	$Co_{0.5}Ni_{0.5}Fe_2O_4$	8.32	37.7nm
3	$Co_{0.5}Zn_{0.5}Fe_2O_4$	8.33	36.08nm
4	$Co_{0.5}Mg_{0.5}Fe_2O_4$	8.41	26.4nm
5	$Co_{0.5}Mn_{0.5}Fe_2O_4$	8.34	30.9nm

4.2 FTIR analysis:

To examine the nature of chemical bonds present in the produced specimen FTIR study was performed in the range of 4000 cm^{-1} to 350 cm^{-1}. The figure shows the FTIR peaks of pure and doped cobalt ferrite.

Sample for FTIR analysis was prepared by homogenous mixing of sample and potassium bromide and then the powder is converted into pellets.

Peaks at 3415-350 cm^{-1} a band observed vibrational stretching frequencies of adsorbed H-O-H or free water molecules. While peaks at 1618-1632 cm^{-1} allocated to C-O bond stretching vibration. The bonds at 1101-1113 cm^{-1} are allocated to Water molecules retained in the prepared samples. The two main peaks at 569-582cm^{-1} and 385-403cm^{-1} are assigned to intrinsic vibrational stretching frequency of Fe-O (tetrahedral sites) and Co-O (octahedral sites) [76] . It can be seen that there is

shift towards higher range for Cobalt Nickel ferrite, Cobalt Zinc ferrite and Cobalt Manganese ferrite which represents a decrease in bond length while shifts towards lower range for Cobalt Magnesium ferrite results in increase in bond length.

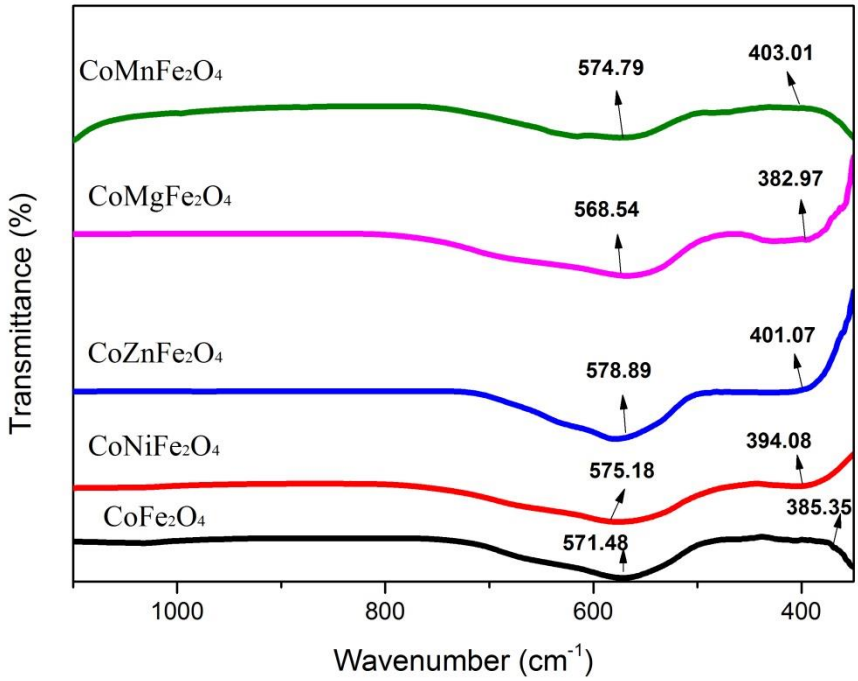

Fig 4.2 FTIR analysis of pure and doped Cobalt Ferrite Nanoparticles

Table 4.2: Tetrahedral (v_1) and Octahedral (v_2) frequency bands of prepared samples

Sample	**v_1 (cm^{-1})**	**v_2 (cm^{-1})**
$CoFe_2O_4$	571	385
$Co_{0.5}Ni_{0.5}Fe_2O_4$	575	394
$Co_{0.5}Zn_{0.5}Fe_2O_4$	578	401
$Co_{0.5}Mg_{0.5}Fe_2O_4$	568	382
$Co_{0.5}Mn_{0.5}Fe_2O_4$	574	403

4.3 SEM analysis:

Scanning electron microscopy was used to study morphological properties and particle size of the material. Suspension of the samples for analysis was prepared using deionized water and sonicate for 3 hours. Fig 4.3 shows the SEM images. The images shows that the sample prepared have spherical uniform distribution while some agglomeration can be seen in some samples due to deprived sonication. Particle size found to be in the range of 26nm to 38nm. EDX analysis shows element composition and mass percentages. EDX confirms the presence of Co, Fe, O, Ni, Zn, Mn and Mg.

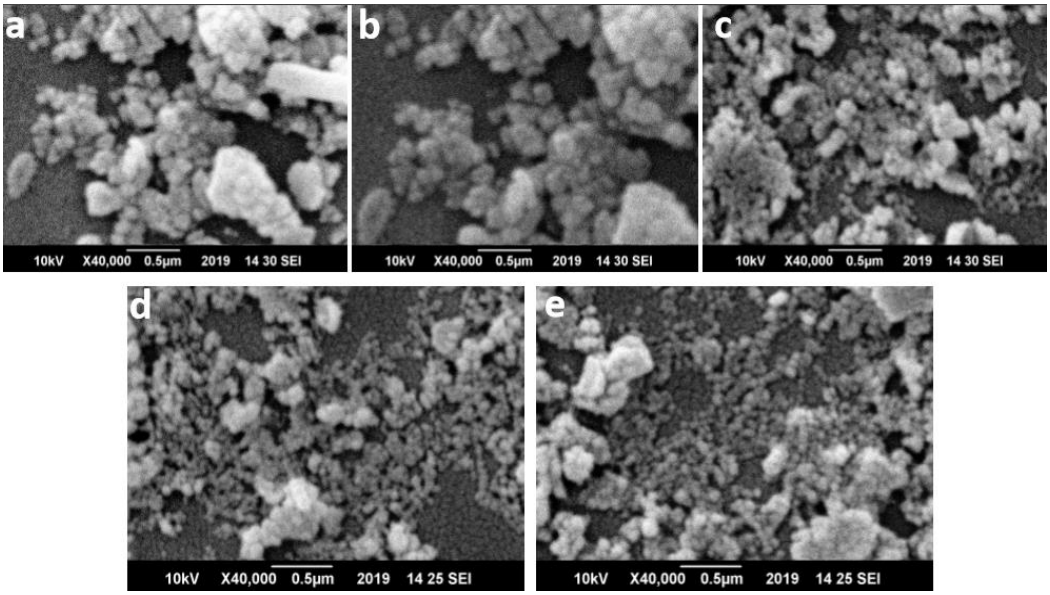

Fig 4.3 SEM images for pure and doped Cobalt Ferrite Nanoparticles (a) Cobalt Ferrite (b) Cobalt Nickel Ferrite (c) Cobalt Zinc Ferrite (d) Cobalt Manganese Ferrite (e) Cobalt Magnesium Ferrite

Table 4.3 Elemental composition of pure and doped Cobalt Ferrite Nanoparticles

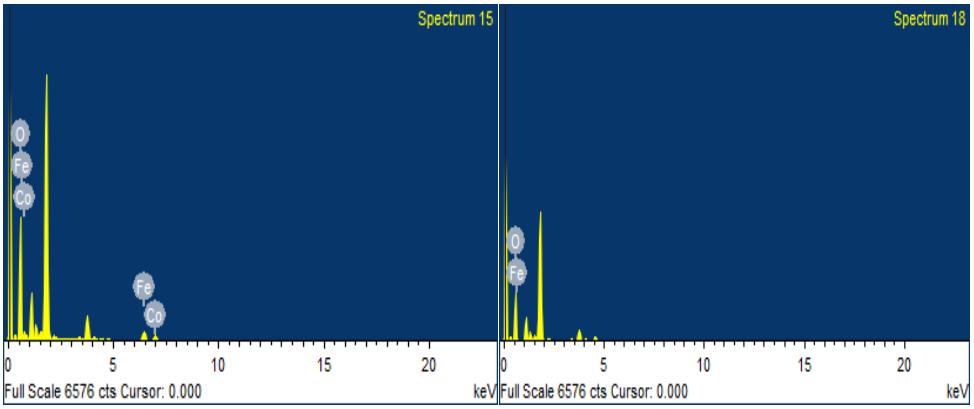

Element	Weight %	Atomic%	Element	Weight%	Atomic%
O K	72.75	90.50	O K	88.36	96.41
Fe K	16.05	5.72	Fe K	8.37	2.62
Co K	11.20	3.78	Co K	2.56	0.76
			Ni K	0.72	0.21
Totals	100.00				
			Totals	100.00	

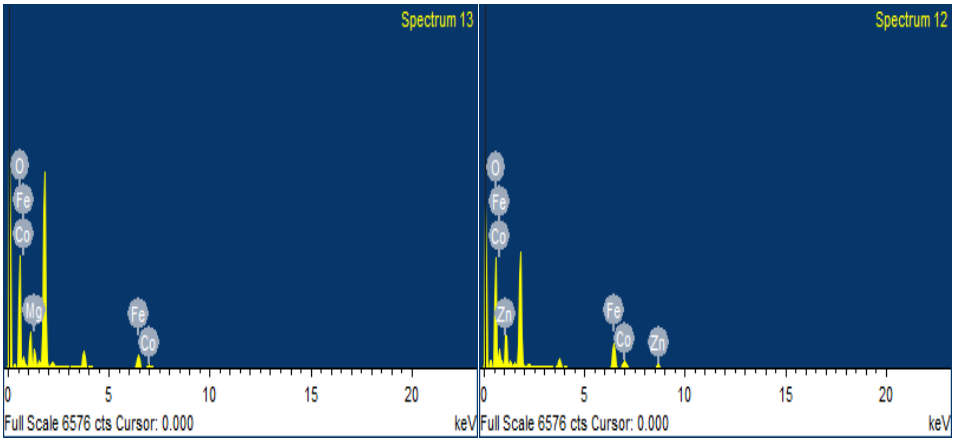

Element	Weight%	Atomic%	Element	Weight%	Atomic%
O K	49.91	78.49	O K	61.38	80.37
Fe K	27.71	12.49	Mg K	10.84	9.34
Co K	9.69	4.14	Fe K	21.00	7.88
Zn K	12.69	4.88	Co K	6.78	2.41
Totals	100.00		Totals	100.00	

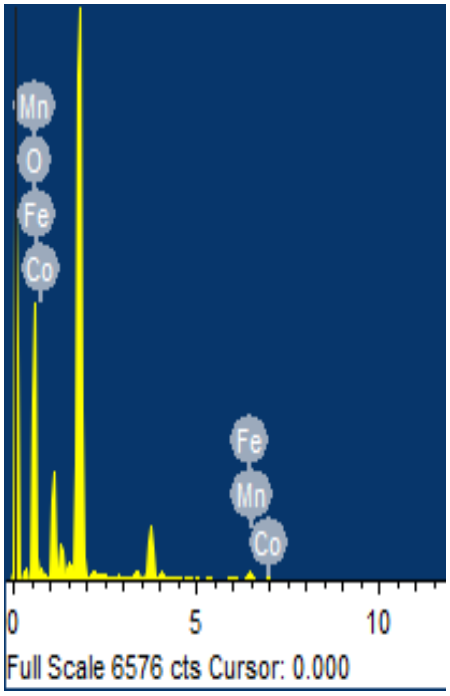

Element	Weight %	Atomic %
O K	87.77	96.20
Mn K	0.56	0.18
Fe K	9.20	2.89
Co K	2.47	0.73
Totals	100.00	

Fig 4.4 EDX for pure and doped Cobalt Ferrite Nanoparticles

4.4 Dielectric studies:

4.4.1 Dielectric Constant:

Dielectric constant of ferrites is represented by ε′ that results in polarization which can either interfacial, dipolar electronic or ionic.

I. Real Part
II. Imaginary Part

Dielectric constant real part depends on the energy storage capabilities of material or polarization. Graph (fig.4.5) the deviation in dielectric constant values along frequency. At each point dielectric constant value is decreasing among frequency and eventually becomes constant. The space charge polarization leads to decreasing trend for dielectric constant. Higher frequency leads to low dielectric constant because of the sudden of applied field the dipole are not able to line up.

According to Maxwell and Wagner model [64] of space charge polarization, dielectric material is divided into parts, grain and grain boundaries. Grain boundaries are highly resistive in nature while grains have conductive nature. Under applied Electric field the electron moves towards grain boundaries and because of resistive nature of boundaries electrons accumulated which leads to polarization.

At low frequency the space charge polarization tends to higher dielectric constant. while at higher frequency values this phenomena becomes slow which leads to decrease in polarization and dielectric constant. [65] while the rise in dielectric constant as shown in fig is due to the substitution of Co^{+2} ions and Fe^{+3} ions with dopant element at tetrahedral site which leads to higher concentration of Fe^{+3} and Fe^{+2} ions at octahedral site and an increase in hopping of electrons between them that leads to increased polarization and dielectric constant.

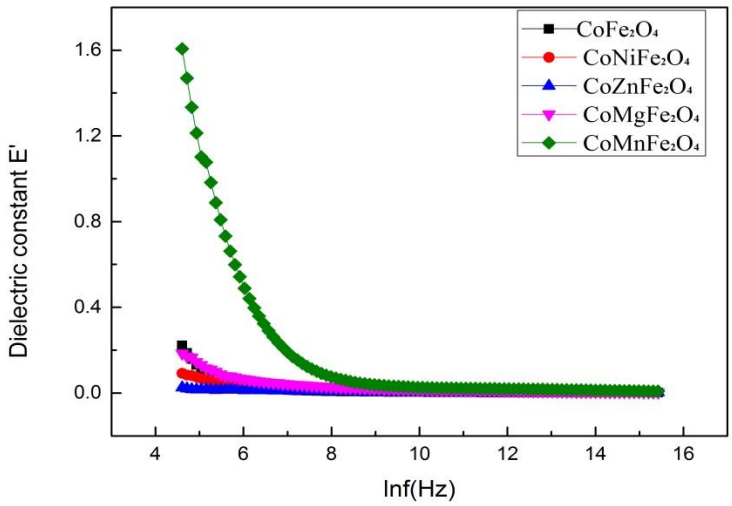

Fig 4.5 Dielectric constant

From fig 4.5 it is observed that dielectric constant for cobalt ferrite when doped with manganese increases while for magnesium, Zinc and Nickel its value decreases.

4.4.2 Dielectric Loss:

Dielectric loss is known as imaginary part that deals with energy dissipation. From the trend shown in fig. 4.6 the dielectric loss decreases with increasing frequency. While the trend is higher for dopant having higher ionic radii than cobalt while lower for the smaller ionic radii than cobalt.

According to Koop's theory, more energy is required for polarization at grain boundaries in low frequency area that leads to more energy losses because of highly resistive grain boundaries. While resistivity in high frequency region is lower so dielectric loss start to decrease. [66]

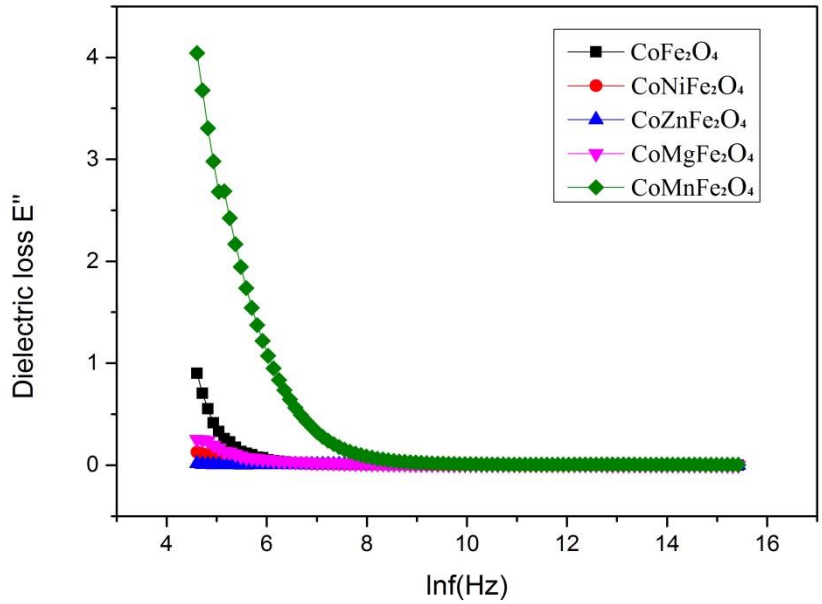

Fig 4.6 Dielectric Loss

As from the figure dielectric loss value against manganese doped cobalt ferrite is higher as compare to cobalt ferrite and decreases with increasing frequency because of its higher ionic radii. While for nickel, zinc and magnesium its value is smaller.

4.4.3 Tangent Loss:

Tangent loss is represented by the ratio of imaginary to real part i.e **ε′′/ε′**. From the figure the tangent loss decreases with increasing frequency because hopping of electron among Fe^{+3} and Fe^{+2} is higher at lower frequency which decreases along frequency and there is decrease in value of tangent loss. Tangent loss takes place when polarization falls behind applied field.

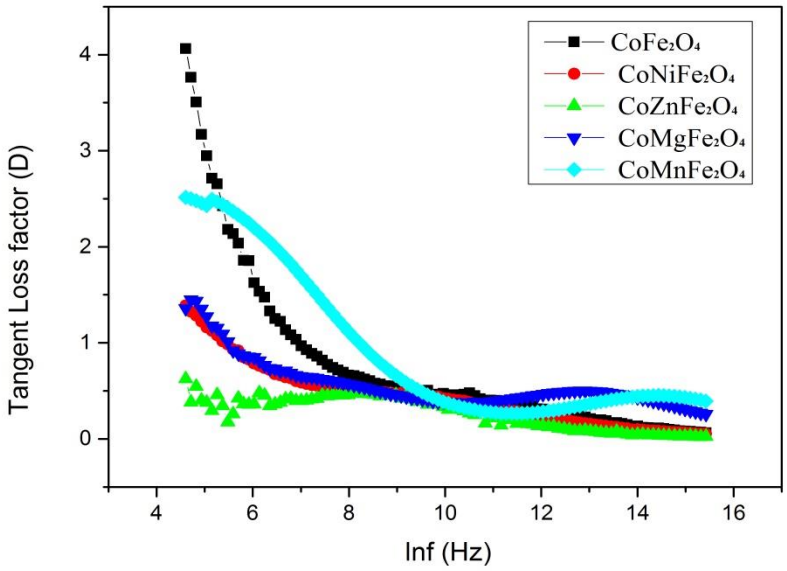

Fig 4.7 Tangent Loss

4.4.4 Ac conductivity:

Ac conductivity deals with the conductive nature of spinel ferrites. From Verwey mechanism this conductivity occurs due to the exchange of electrons among the ions of the similar component existing in more than one valence state at octahedral site.

The Ac conductivity is given by

$$\sigma_{ac} = \omega \varepsilon_o \varepsilon''$$

Where $\omega=2\pi f$, f represented the frequency, ε_o represents the permittivity of free space and ε'' represents dielectric loss.

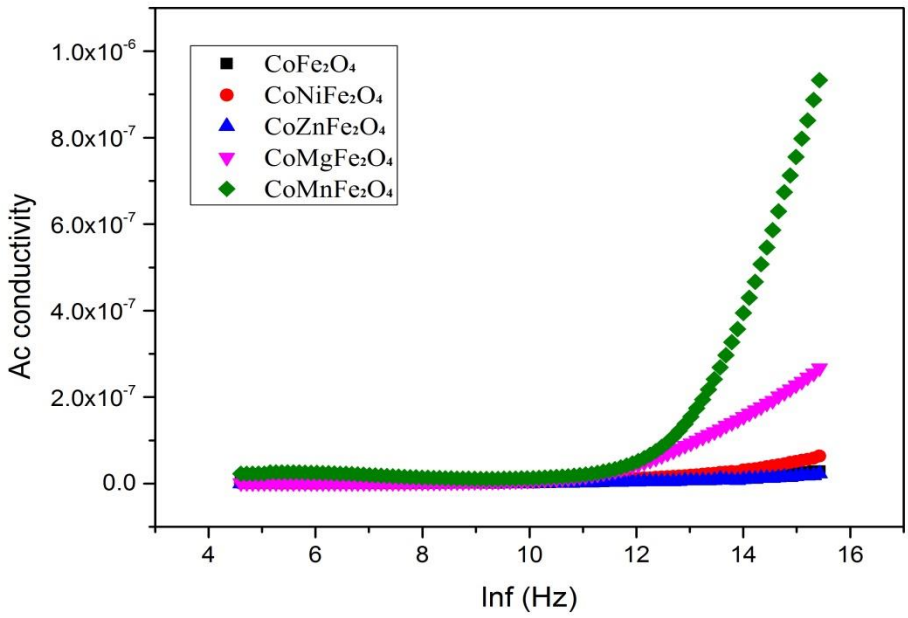

Fig 4.8 Ac conductivity

From the graph Ac conductivity increases along increasing frequency and have lower values within low frequency region. From Maxwell Wagner conductivity is low at grain boundaries due to resistivity while when frequency increases the electron movement increase which leads to increase in ac conductivity at grain due to increase in electron hopping.

4.4.5 Ac Impedance:

Both real and imaginary parts are calculated at room temperature. The complex part deals with the interactions at grain and grain boundaries. Real part deals with frequency based variation in resistive part while imaginary part deals with frequency based variation in reactive part of the impedance. The graph shows a decreasing trend in Ac impedance along frequency. There is decreasing trend because of enhanced conductivity of the material. The space charge polarization value decreases at higher frequency which leads to constant impedance. While because of high space charge polarization value in low frequency range impedance is lower.

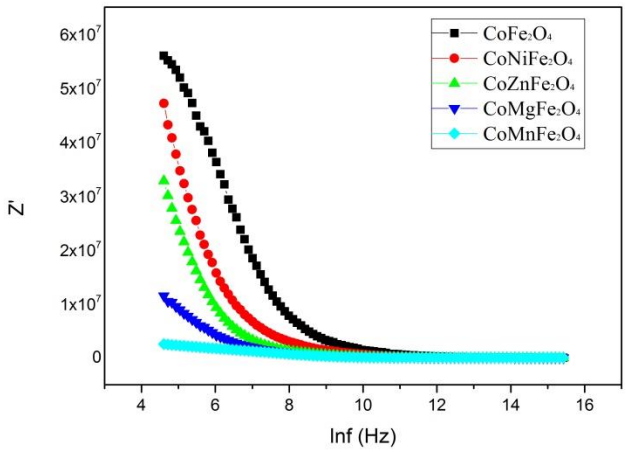

(a)

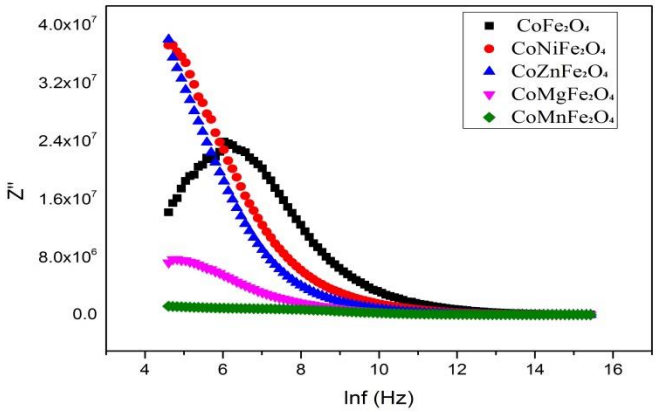

(b)

Fig 4.9 Ac impedance (a) real part (z′) (b) imaginary part (z′′)

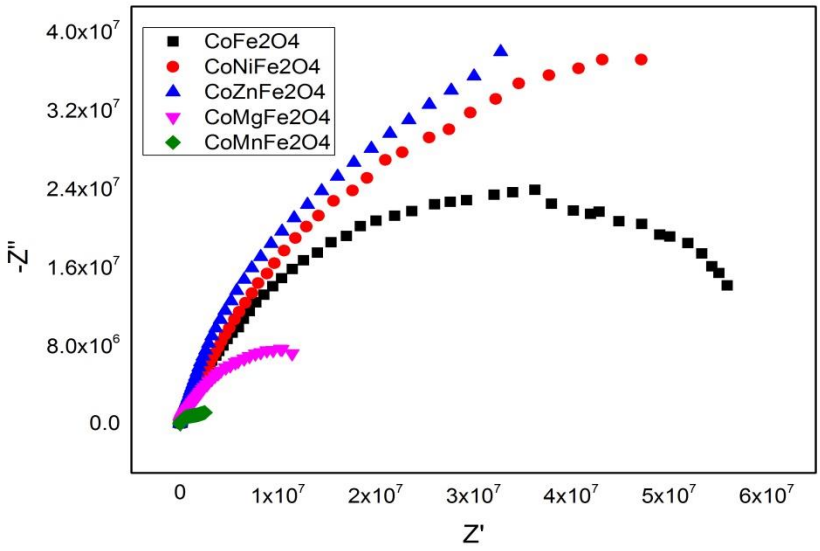

Fig 4.10 Cole-Cole plot (z′ vs z″)

Fig 4.10 represents the cole-cole (Z′ vs Z″) plot for Cobalt ferrite and doping. Semi curved trends represent different composition at different frequencies. From Cole-Cole curves we can analyse the resistance effect of grain, grain boundaries, sample-electrode effect, defects and relaxation process. Cole – Cole trend with these semicircles shows a relaxation process and resistance of the material can be calculated by radius of semicircle, having Debye-type conduction. While conduction of non-debye type depressed semicircle appears. Mostly for the cole-cole plot three different semicircles appears, semicircles at low frequency range are related to resistance of grain boundaries, usually grain boundaries contains structural and chemical effects which results in more resistance than bulk. While, the semicircle which lies in high frequency range are related to interior resistive grain effect and third semicircle range is related to electrode effect. [67]

4.4.6 Complex Electric modulus:

Analyzation of Electrical behaviour of a material can be studied through complex electric modulus. Sample polycrystalline nature (homogenous and inhomogeneous) and these materials microscopic property electrical relaxation of

ionic solids can be studied using this method. For M(f) there is a wide tilted peak in the imaginary part while in real part there is sigmoidal curve.

From the figure it is shown that along low frequency range M′ is excessively small along with increasing frequency its value increases and approaches to maximum asymptotic value for all samples. This trend relates to the mobility of charge carrier which are govern by restoring force under the applied field. Charge carriers with long- range mobility tends to cause electrode polarization while high range frequency leads to short range mobility of charge carrier which results in conduction phenomena (specially due to ion mobility).

From Imaginary component of modulus (M″) inclusive data is concluded about charge transport as frequency dependent. From the figure the peaks in the low frequency region indicates space where ion travel through long distance, i.e., ion transfer from one site to other. While in higher frequency area the ions are confined to their potential well so they can move within the well. With the increase in frequency graph shows transition from long-range to short range mobility.

The broad nature of peaks shows distributions of relaxation time because of non-Debye nature of the sample. While the modulus spectrum peaks clearly shows the conductivity relaxation. With the increasing frequency the relaxation time increases.

From fig 4.11 (M’ vs. M’’) single phase is confirmed and the semicircles indicates the non-Debye type of relaxation in the material.[78]

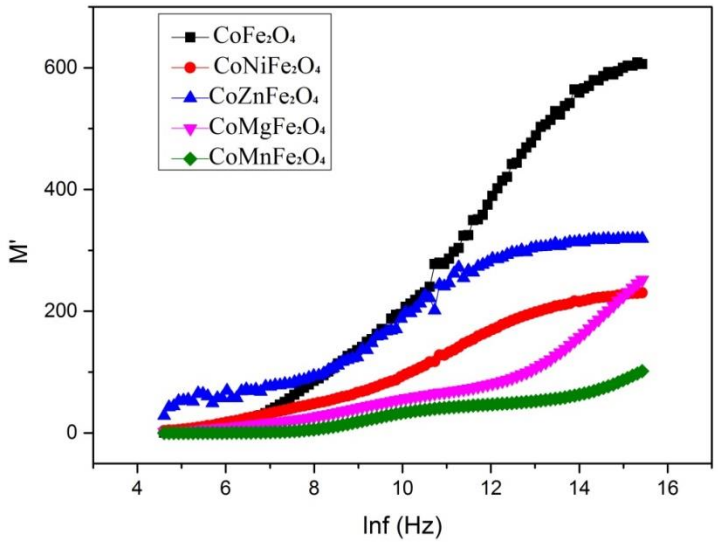
CoFe₂O₄
CoNiFe₂O₄
CoZnFe₂O₄
CoMgFe₂O₄
CoMnFe₂O₄
M'
lnf (Hz)

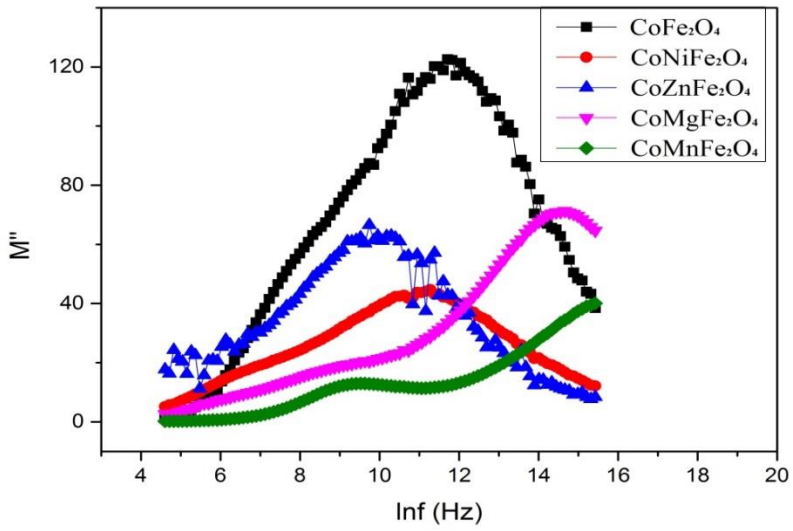
CoFe₂O₄
CoNiFe₂O₄
CoZnFe₂O₄
CoMgFe₂O₄
CoMnFe₂O₄
M''
lnf (Hz)

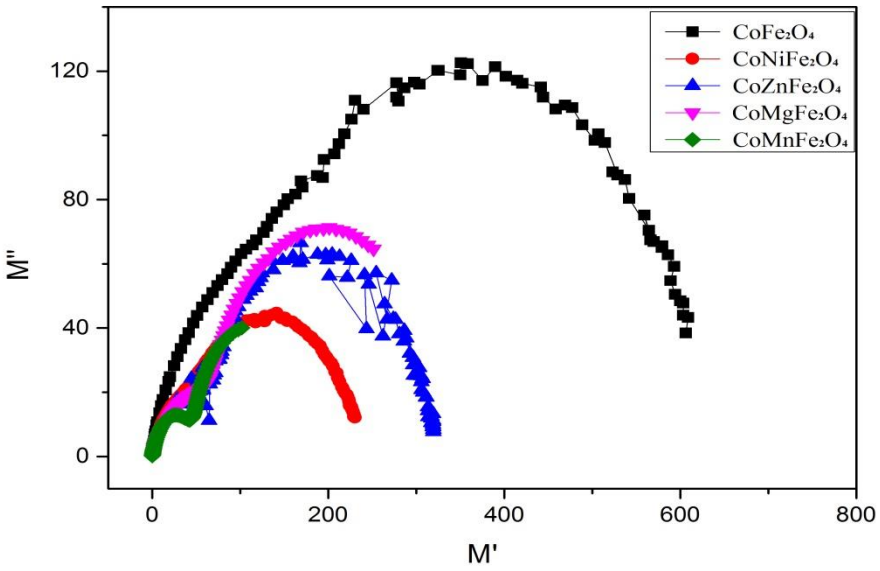

Fig 4.11 Electric Modulus

4.5 Magnetic measurements:

Vibrating Sample Magnetometer (VSM) is a approach used for magnetic measurements. This is used to measure M-H loop for pure cobalt ferrite and Manganese doped Cobalt ferrite up to magnetic field of 10kOe as shown in fig. [68]

In spinel family of ferrites due to the interaction and exchange of metals ions at octahedral and tetrahedral site they possesses a net magnetic order. Generally , in reverse spinel ferrite structure 8 divalent metal ions (Mn^{2+}) settled on octahedral site while 16Fe^{3+} ions are equally allocated between both sites.[79]

$$(\downarrow M^{2+} \downarrow Fe^{3+})_B (\uparrow Fe^{3+})_A O_4^{2-}$$

From fig 4.12 it is concluded that cobalt ferrite is a nearly a soft magnetic material. While the coercivity values of the material depends upon the grain sizes.

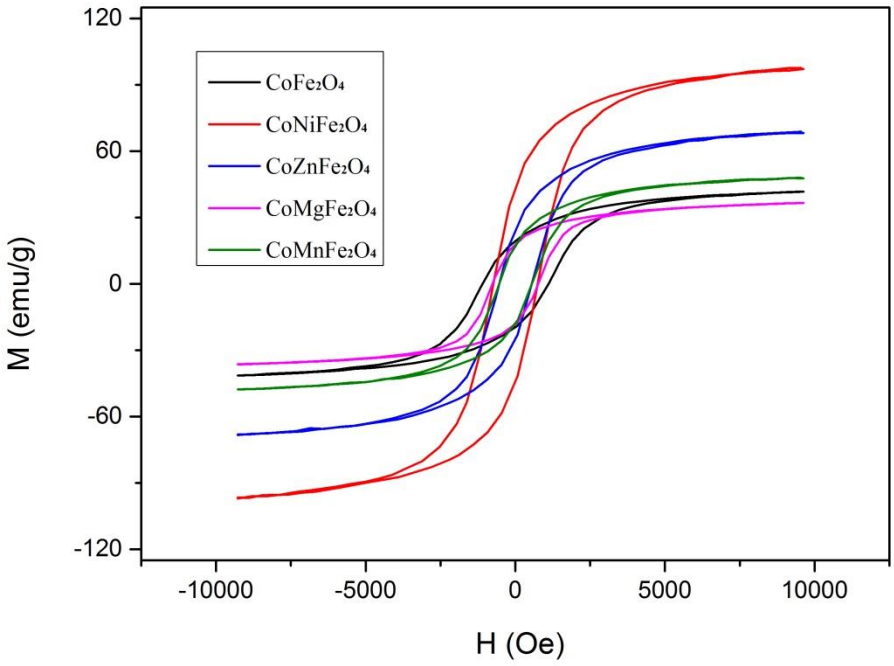

Fig 4.12 Hysteresis loop for pure and doped Cobalt Ferrite Nanoparticles

When Cobalt ferrite is doped with metallic cations, result in increase of total magnetic moments. Hence, the net saturation magnetization is increased. So Ms=41.6emu/g for pure Cobalt ferrite, and maximum for Cobalt nickel ferrite Ms=97.16 emu/g. while for magnesium ferrite its value is decreases (M_s=36.52). Similarly, the value of remanence magnetization Mr can also be calculated using VSM result. For pure Cobalt ferrite, the Mr= 19.34emu/g. while its value increases for Cobalt Nickel ferrite and Cobalt Zinc ferrite (43.32 emu/g , 24.34 emu/g). While decreases for Cobalt magnesium ferrite and Cobalt Manganese ferrite (17.9 emu/g, 17.34 emu/g) . The **Coercivity** value increases for the dopants as compare to pure cobalt ferrite.

Table 4.4 : Values of Saturation Magnetization, Remanence and Coercivity of Pure and Doped Cobalt Ferrite Nanoparticles

Sample	**M_s (emu/g)**	**M_r (emu/g)**	**H_c (Am^{-1})**
$CoFe_2O_4$	41.6	19.34	87533.22
$CoNiFe_2O_4$	97.16	43.32	58084.39
$CoZnFe_2O_4$	68.26	24.34	43051.49
$CoMgFe_2O_4$	36.52	17.9	60846.68
$CoMnFe_2O_4$	47.84	17.34	43492.91

CONCLUSIONS:

The pure and doped Cobalt ferrite was successfully prepared from Sol-Gel method. XRD pattern of $Co_{0.5}(M_{0.5})Fe_2O_4$ (M= Ni, Zn, Mg and Mn) proves that all the specimen have single cubic phase composition. No contamination found in the synthesized material. Crystallite size was found using Scherer equation which lies within the range of 26-38 nm. SEM specifically shows that nanoparticles were well made, spherical in appearance and there was little agglomeration noted. The images of Sem show the particles to be spherical and less agglomerated as the dopant concentration increases. FTIR studies indicates existence of metal -oxygen bonds in both sites of the ferrites and with the addition of dopants, band shifts proceeding to lower and higher frequency range. From LCR meter dielectric measurements of the samples were studied. Dielectric constant shows higher values in lower frequency region while decreases along increasing frequency. AC conductivity shows an increasing trend along frequency . The value for Cobalt manganese ferrite is higher because of its higher ionic radii. All the dielectric results shows a relation with the Maxwell-Wagner model and Koop's theory. Vibrating sample magnetometer (VSM) was used to analyze the magnetic measurements. From VSM measurements it is recognized that the saturation magnetization increases for $CoNiFe_2O_4$, $CoZnFe_2O_4$ and $CoMnFe_2O_4$ because of higher ionic radii while decreases for $CoMgFe_2O_4$. Ms increases for $CoNiFe_2O_4$ and $CoZnFe_2O_4$ while decreases for $CoMgFe_2O_4$ and $CoMnFe_2O_4$. Magnetic Coercivity studies of the pure and doped sample revealed a decrease in the value of coercivity with dopant.

Future Work:

The composite with different polymers can be made in order to study different properties including mechanical, electrical and optical properties.

References:

[1] Baig, M. M., Pervaiz, E., & Afzal, M. J. (2020). Catalytic activity and kinetic studies of Core@ Shell nanostructure $NiFe_2O_4$@ TiO_2 for photocatalytic degradation of methyl orange dye. *J. Chem. Soc. Pak*, *42*(04), 531.

[2] Heyn, E. (1912). Rapport sur les progrès de la Métallographie depuis le commencement de l'année 1909 jusqu'à la fin de l'année (1911). *Revue de Métallurgie*, *9*(12), 934-982.

[3] Ederer, C. and N.A. Spaldin, Weak ferromagnetism and magnetoelectric coupling in bismuth ferrite. Physical Review B, 2005. 71(6): p. 060401.

[4] ur Rahman, O., S.C. Mohapatra, and S. Ahmad, Fe $_3$ O $_4$ inverse spinal super paramagnetic nanoparticles. Materials Chemistry and Physics, (2012). 132(1): p. 196-202.

[5] Heck, C., Magnetic materials and their applications. (2013): Elsevier

[6] Snoek, J. L. (1936). Magnetic and electrical properties of the binary systems MO. Fe_2O_3. *Physica*, *3*(6), 463-483.

[7] Néel, L. (1952). Antiferromagnetism and ferrimagnetism. *Proceedings of the Physical Society. Section A*, *65*(11), 869.

[8] Koops, C. G. (1951). On the dispersion of resistivity and dielectric constant of some semiconductors at audiofrequencies. *Physical review*, *83*(1), 121.

[9] Chen, C. W. (2013). *Magnetism and metallurgy of soft magnetic materials*. Courier Corporation.

[10] Yeadon, W. H., & Yeadon, A. (2001). *Handbook of small electric motors*. McGraw Hill Professional.

[11] Bragg, W. H. (1915). XXX. The structure of the spinel group of crystals. *The London, Edinburgh, and Dublin Philosophical Magazine and Journal of Science*, *30*(176), 305-315.

[12] Gorter, E. W. (1954). Saturation magnetization and crystal chemistry of ferrimagnetic oxides. I. II. Theory of ferrimagnetism. *Philips Res. Rep.*, *9*, 295-320.

[13] Clarricoats Microwave ferrites. (1961): Wiley.

[14] Barth, T. F., & Posnjak, E. (1932). Spinel structures: with and without variate atom equipoints. *Zeitschrift Für Kristallographie-Crystalline Materials*, *82*(1-6), 325-341.

[15] Mathew, D.S. and R.-S. Juang, An overview of the structure and magnetism of spinel ferrite nanoparticles and their synthesis in microemulsions. Chemical Engineering Journal, 2007. 129(1): p. 51-65

[16] Gomes, J. A., Sousa, M. H., Tourinho, F. A., Mestnik-Filho, J., Itri, R., & Depeyrot, J. (2005). Rietveld structure refinement of the cation distribution in ferrite fine particles studied by X-ray powder diffraction. *Journal of magnetism and magnetic materials*, *289*, 184-187.

[17] Mittal, V. K., Chandramohan, P., Bera, S., Srinivasan, M. P., Velmurugan, S. V. N. S., & Narasimhan, S. V. (2006). Cation distribution in $Ni_xMg_{1-x}Fe_2O_4$ studied by XPS and Mössbauer spectroscopy. *Solid state communications*, *137*(1-2), 6-10.

[18] Amer, M., Ata-Allah, S., Meaz, T., Aboul-Enein, S., & Abd-El-Hamid, M. (2005). Mössbauer, Infrared and X-ray Studies for Ni_ {0.5} Zn_ {0.5} Cr_xFe_ {2-x} O_4 Ferrites. *Turkish Journal of Physics*, *29*(3), 163-177.

[19] Brockhouse, B., BN Brockhouse, LM Corliss, and JM Hastings, Phys. Rev. 98, 1721 (1955). Phys. Rev., (1955). 98: p. 1721.

[20] D. S. Mathew and R.-S. Juang, "An overview of the structure and magnetism of spinel ferrite nanoparticles and their synthesis in microemulsions," Chemical engineering journal, vol. 129, pp. 51-65, (2007).

[21] S. Anjum, A. Rashid, F. Bashir, S. Riaz, M. Pervaiz, and R. Zia, "Effect of Cu-doped nickel ferrites on structural, magnetic, and dielectric properties," IEEE Transactions on Magnetics, vol. 50, pp. 1-4, (2014).

[22] D. Li and R. B. Kaner, "Graphene-based materials," Nat Nanotechnol, vol. 3, p. 101, (2008).

[23] K. V. Babu, G. Satyanarayana, B. Sailaja, G. S. Kumar, K. Jalaiah, and M. Ravi, "Structural and magnetic properties of $Ni_{0.8}M_{0.2}Fe_2O_4$ (M= Cu, Co) nano-crystalline ferrites," Results in Physics, vol. 9, pp. 55-62, (2018).

[24] P. Yin, Y. Deng, L. Zhang, W. Wu, J. Wang, X. Feng, "One-step hydrothermal synthesis and enhanced microwave absorption properties of $Ni0.5Co_{0.5}Fe_2O_4$/graphene composites in low frequency band," Ceramics International, vol. 44, pp. 20896-20905, (2018)

[25] S. A. Soomro, I. H. Gul, M. Z. Khan, H. Naseer, and A. N. Khan, "Dielectric properties evaluation of $NiFe_2O_4$/MWCNTs nanohybrid for microwave applications

prepared via novel one step synthesis," Ceramics International, vol. 43, pp. 4090-4095, (2017).

[26] P. A. Noorkhan and S. Kalayne, "Synthesis, Characterization Ac Conductivity of Nickel Ferrite," Journal of Engineering Research and Applications, vol. 2, pp. 681-685, (2012). 68

[27] V. V. Dhole, "INTERNATIONAL JOURNAL OF ENGINEERING SCIENCES & RESEARCH TECHNOLOGY STRUCTURAL AND MAGNETIC PROPERTIES OF NICKEL FERRITE NANOPARTICLES BY WET CHEMICAL CO-PRECIPITATION TECHNIQUE."

[28] J. Haspers, "Ferrites: Their Properties and Applications," in Modern Materials. vol. 3, ed: Elsevier, (1962), pp. 259-341.

[29] S. Akhter, D. P. Paul, M. A. Hakim, D. K. Saha, M. Al-Mamun, and A. Parveen, "Synthesis, structural and physical properties of Cu1–xZnxFe2O4 ferrites," Materials Sciences and Applications, vol. 2, p. 1675, (2011).

L. Zhang, X. Yu, H. Hu, Y. Li, M. Wu, Z. Wang, "Facile synthesis of iron oxides/reduced graphene oxide composites: application for electromagnetic wave absorption at high temperature," Scientific reports, vol. 5, p. 9298, (2015).

[30] Singh, C., Jauhar, S., Kumar, V., Singh, J., & Singhal, S. (2015). Synthesis of zinc substituted cobalt ferrites via reverse micelle technique involving in situ template formation: a study on their structural, magnetic, optical and catalytic properties. *Materials Chemistry and Physics*, *156*, 188-197.

[31] Manikandan, A., Vijaya, J. J., Sundararajan, M., Meganathan, C., Kennedy, L. J., & Bououdina, M. (2013). Optical and magnetic properties of Mg-doped $ZnFe_2O_4$ nanoparticles prepared by rapid microwave combustion method. *Superlattices and Microstructures*, *64*, 118-131.

[32] Singh, C., Goyal, A., & Singhal, S. (2014). Nickel-doped cobalt ferrite nanoparticles: efficient catalysts for the reduction of nitroaromatic compounds and photo-oxidative degradation of toxic dyes. *Nanoscale*, *6*(14), 7959-7970.

[33] Singh, S., & Singhal, S. (2019). Transition metal doped cobalt ferrite nanoparticles: efficient photocatalyst for photodegradation of textile dye. *Materials Today: Proceedings*, *14*, 453-460.

[34] Kumar, P., Sharma, S. K., Knobel, M., & Singh, M. (2010). Effect of La^{3+} doping on the electric, dielectric and magnetic properties of cobalt ferrite processed by co-precipitation technique. *Journal of Alloys and Compounds*, *508*(1), 115-118.

[35] Bhukal, S., & Singhal, S. (2014). Magnetically separable copper substituted cobalt–zinc nano-ferrite photocatalyst with enhanced photocatalytic activity. *Materials science in semiconductor processing*, *26*, 467-476.

[36] Naik, M. M., Naik, H. B., Nagaraju, G., Vinuth, M., Vinu, K., & Viswanath, R. (2019). Green synthesis of zinc doped cobalt ferrite nanoparticles: Structural, optical, photocatalytic and antibacterial studies. *Nano-Structures & Nano-Objects*, *19*, 100322.

[37] Chandel, S., Thakur, P., Tomar, M., Gupta, V., & Thakur, A. (2017). Investigation of structural, optical, dielectric and magnetic studies of Mn substituted $BiFeO_3$ multiferroics. *Ceramics International*, *43*(16), 13750-13758.

[38] Tatarchuk, T. R., Paliychuk, N. D., Bououdina, M., Al-Najar, B., Pacia, M., Macyk, W., & Shyichuk, A. (2018). Effect of cobalt substitution on structural, elastic, magnetic and optical properties of zinc ferrite nanoparticles. *Journal of Alloys and Compounds*, *731*, 1256-1266.

[39] Wu, X., Ding, Z., Song, N., Li, L., & Wang, W. (2016). Effect of the rare-earth substitution on the structural, magnetic and adsorption properties in cobalt ferrite nanoparticles. *Ceramics International*, *42*(3), 4246-4255.

[40] Padmapriya, G., Manikandan, A., Krishnasamy, V., Jaganathan, S. K., & Antony, S. A. (2016). Spinel $Ni_xZn_{1-x}Fe_2O_4$ ($0.0 \leq x \leq 1.0$) nano-photocatalysts: synthesis, characterization and photocatalytic degradation of methylene blue dye. *Journal of Molecular Structure*, *1119*, 39-47.

[41] Moradmard, H., Shayesteh, S. F., Tohidi, P., Abbas, Z., & Khaleghi, M. (2015). Structural, magnetic and dielectric properties of magnesium doped nickel ferrite nanoparticles. *Journal of Alloys and Compounds*, *650*, 116-122.

[42] Qindeel, R., & Alonizan, N. H. (2018). Structural, dielectric and magnetic properties of cobalt based spinel ferrites. *Current Applied Physics*, *18*(5), 519-525.

[43] Satar, N. S. A., Adnan, R., Lee, H. L., Hall, S. R., Kobayashi, T., Kassim, M. H. M., & Kaus, N. H. M. (2019). Facile green synthesis of ytrium-doped $BiFeO_3$ with highly efficient photocatalytic degradation towards methylene blue. *Ceramics International*, *45*(13), 15964-15973.

[44] Abraham, A. G., Manikandan, A., Manikandan, E., Vadivel, S., Jaganathan, S. K., Baykal, A., & Renganathan, P. S. (2018). Enhanced magneto-optical and photo-catalytic properties of transition metal cobalt (Co2+ ions) doped spinel $MgFe_2O_4$ ferrite nanocomposites. *Journal of Magnetism and Magnetic Materials*, *452*, 380-388.

[45] J. Huang, F. Xie, C. Wang, and Z. Mao, "Development of solid oxide fuel cell materials for intermediate-to-low temperature operation," Int. J. Hydrogen Energy, vol. 37, pp. 877-883, (2012).

[46] A. J. Jacobson, "Materials for solid oxide fuel cells," Chem. Mater., vol. 22, pp. 660-674, (2010).

[47] V. Kharton, F. Marques, and A. Atkinson, "Transport properties of solid oxide electrolyte ceramics: a brief review," Solid State Ionics vol. 174, pp. 135-149, (2004)

[48] H. Okkay, M. Bayramoglu, and M. F. Öksüzömer, "$Ce_{0.8}Sm_{0.2}O_{1.9}$ synthesis for solid oxide fuel cell electrolyte by ultrasound assisted co-precipitation method," Ultrason. Sonochem, vol. 20, pp. 978-983, 2013.

[49] Y. P. Fu, S. B. Wen, and C. H. Lu, "Preparation and characterization of samaria-doped ceria electrolyte materials for solid oxide fuel cells," J. Am. Ceram. Soc., vol. (2007), pp. 127-131, 2007.

[50] Lerouge, F., G. Cerveau, and R.J. Corriu, Supramolecular self-organization in non-crystalline hybrid organic–inorganic nanomaterials induced by van der Waals interactions. New Journal of Chemistry, (2006). 30(10): p. 1364-1376.

[51] Samoila, P., Slatineanu, T., Postolache, P., Iordan, A. R., & Palamaru, M. N. (2012). The effect of chelating/combustion agent on catalytic activity and magnetic

properties of Dy doped Ni–Zn ferrite. *Materials Chemistry and Physics*, *136*(1), 241-246.

[52] Druc, A. C., Dumitrescu, A. M., Borhan, A. I., Nica, V., Iordan, A. R., & Palamaru, M. N. (2013). Optimization of synthesis conditions and the study of magnetic and dielectric properties for $MgFe_2O_4$ ferrite. *Central European Journal of Chemistry*, *11*(8), 1330-1342.

[53] Shirsath, S. E., Mane, M. L., Yasukawa, Y., Liu, X., & Morisako, A. (2013). Chemical tuning of structure formation and combustion process in $CoDy_{0.1}Fe_{1.9}O_4$ nanoparticles: influence@ pH. *Journal of nanoparticle research*, *15*(10), (1976).

[54] J. W. Niemantsverdriet, "Spectroscopy in Catalysis," vol. 3, pp. 147-175, 179212, (2007).

[55] A. I. Kirkland and J. L. Hutchison, "Nanocharacterisation," vol. 1, (2007).

[56] Thermo, N., Introduction to Fourier transform infrared spectrometry. Thermo Nicolet Corporation: Madison-USA, (2001)

[57] Zhang, X., Sun, X., Chen, Y., Zhang, D., & Ma, Y. (2012). One-step solvothermal synthesis of graphene/Mn3O4 nanocomposites and their electrochemical properties for supercapacitors. *Materials Letters*, *68*, 336-339.

[58] J. W. Niemantsverdriet, "Spectroscopy in Catalysis," vol. 3, pp. 147-175, 179212, (2007).

[59] A. I. Kirkland and J. L. Hutchison, "Nanocharacterisation," vol. 1, (2007)

[61] B. Faust, "Modern Chemical Techniques," Royal Society of Chemistry, vol. 1, pp. 92-115, (2012).

[62] B. &. V. B. Kirupakar, "Vibrating sample magnetometer and its application in characterisation of magnetic property of the anti cancer drug magnetic microspheres," *International Journal of pharmaceutics and Drug Analysis, (*2016).

[63] T. S. Tripathi, "Electronic transport and magnetic properties of chromium chalcogenide spinels: CuCr2X4 (X== S, Se, Te) and Cu1+. TCr2Te4 (x== 0-1)," (2011).

[64] A. Samavati and A. F. Ismail, “Antibacterial properties of copper-substituted cobalt ferrite nanoparticles synthesized by co-precipitation method,” *Particuology*, vol. 30, pp. 158–163, (2017).

[65] Yadav, G., Kumar, N., Shah, J., Kotnala, R. K., & Aggrawal, R. Enhancement in Magnetic and Dielectric Properties of Magnesium Ferrite by Lithium Substitution Applicable for High Frequency Shielding Material.

[66] Sharma, J., Sharma, N., Parashar, J., Saxena, V. K., Bhatnagar, D., & Sharma, K. B. (2015). Dielectric properties of nanocrystalline Co-Mg ferrites. *Journal of Alloys and Compounds*, *649*, 362-367.

[67] Kumari, R., Ahlawat, N., Agarwal, A., Sanghi, S., Sindhu, M., & Ahlawat, N. (2016). Rietveld refinement, impedance spectroscopy and magnetic properties of

$Bi_{0.8}Sr_{0.2}FeO_3$ substituted $Na_{0.5}Bi_{0.5}TiO_3$ ceramics. *Journal of Magnetism and Magnetic Materials*, *414*, 1-9.

[68] S. Farooq, "Farooq, S. (2010). Study of electrical and magnetic properties of strontium-barium hexaferrite nanomaterials for potential technological applications," (2010).

[69] https://qsstudy.com/physics/ferromagnetism

[70] https://www.researchgate.net/figure/The-configuration-of-atomic-dipole-for-an-antiferromagnetism_fig22_265472011

[71] https://www.researchgate.net/figure/The-schematic-representation-of-the-top-down-and-bottom-up-approaches-for-the-fabrication_fig2_324539610

[72] https://www.researchgate.net/figure/schematic-diagram-of-scanning-electron-microscope-SEM_fig14_281097535

[73]https://www.researchgate.net/figure/Schematic-diagram-of-FTIR_fig4_292788248

[74] https://www.cefns.nau.edu/geology/malabs/Microprobe/EDS-EDSvsWDS.html

[75]https://www2.chemistry.msu.edu/faculty/reusch/virttxtjml/spectrpy/uv-vis/spectrum.htm

[76]file:///E:/PROJECT/Research%20articles/Photocatalytic/1-s2.0-S2352507X19300575-main.pdf

[78]file:///E:/PROJECT/Research%20articles/10.1080@00150193.2016.1137467.pdf

[79] Khan, M. Z., Gul, I. H., Baig, M. M., & Khan, A. N. (2020). Comprehensive study on structural, electrical, magnetic and photocatalytic degradation properties of Al^{3+} ions substituted nickel ferrites nanoparticles. *Journal of Alloys and Compounds*, *848*, 155795.